ADDIS ABABA UNIVERSITY
SHOOL OF GRADUATE STUDIES
FACULTY OF TECHNOLOGY

DEPARTMENT OF ELECTRICAL AND COMPUTER ENGINEERING

Comparative Study on The Performance of Wavelet-Based and DFT-Based MCM

A thesis submitted to the School of Graduate Studies of Addis Ababa University in partial fulfillment of the requirements of the Degree of Master of Science in Electrical Engineering

By

Sinshaw Bekele

Advisor - Dr.-Ing. Hailu Ayele

January 2007

ADDIS ABABA UNIVERSITY
SHOOL OF GRADUATE STUDIES
FACULTY OF TECHNOLOGY

Comparative Study on The Performance of
Wavelet-Based and DFT-based MCM

By

Sinshaw Bekele

APPROVAL BY BOARD OF EXAMINERS

Chairman of Department Graduate Committee	Signature
Advisor	Signature
Internal Examiner	Signature
External Examiner	Signature

Abstract

The demand for wireless networks has been growing rapidly over the recent past due to improved reliability, higher supported data rates, seamless connectivity between users and the access point, and low deployment costs relative to wireline infrastructure. This increase in demand started with the popular IEEE 802.11b wireless local area network standard.

Many recent wireless network standards are now employing DFT based multicarrier modulation (MCM) popularly termed as OFDM in their design. Multicarrier modulation reduces the system's susceptibility to the frequency selective fading channel, due to multipath propagation, by transforming it into a collection of approximately flat subchannels. As a result, this makes it easier to compensate for the distortion introduced by the channel. The effects of the Intersymbol Interference (*ISI*) and Intercarrier Interference (*ICI*) are reduced by the application of cyclic prefix. On the other hand, related research in wavelets points that due to the high spectral containment of wavelet filters the performance of MCM improves.

This thesis work investigates simulation based performance of the DFT-based and Wavelet-based MCM. The channel model and system models for both MCM schemes are considered. And using bit error rate (BER) versus signal-to-noise ratio (SNR) as measure of performance, transmission scenarios are implemented in AWGN channel and time varying multipath channel models and studied. Channel coding performances and the effects of carrier frequency offset are investigated.

The performance results obtained by the simulation indicate that the wavelet-based implementation outperforms that of DFT-based in some channel scenarios. While in other channel models the DFT-based MCM shows increased performance.

Acknowledgement

It has been a real privilege and challenge working on this thesis study, and thanks are due for many for its completion. First and for most thanks are due for my advisor Dr.-Ing. Hailu Ayele for his support, guidance and most of all his invaluable insights. It has been a great honor working with him.

I would like to take this opportunity to express my thanks to my family and specially my sister Frehiwot Bekele for her unwaning support throughout this entire experience. And a special thanks goes to Sentayehu Challa, member of the ECE department, for the assistance and resources he provided untiringly.

CONTENTS

Acronyms

ADSL	Asymmetric Digital Subscriber Line
AWGN	Additive White Gaussian Noise
BER	Bit Error Rate
CIR	Channel Impulse Response
CWT	Continuous Wavelet Transform
DAB	Digital Audio Broadcasting
DFT	Discrete Fourier Transform
DMT	Discrete Multitone
DVB	Digital Video Broadcasting
DWT	Discrete Wavelet Transform
FFT	Fast Fourier Transform
ICI	Intercarrier Interference
IEEE	Institute of Electrical and Electronic Engineers
IFFT	Inverse Fast Fourier Transform
ISI	Intersymbol Interference
MCM	Multicarrier Modulation
MRA	Multiresolution Analysis
OFDM	Orthogonal Frequency Division Multiplexing
QAM	Quadrature Amplitude Modulation
SNR	Signal-to-Noise Ratio
STFT	Short-Time Fourier Transform
VDSL	Very high data rate Digital Subscriber Line
WLAN	Wireless Local Area Network
WMAN	Wireless Metropolitan Area Network
WSSUS	Wide-Sense-Stationary Uncorrelated Scattering

List of Figures

List Of Tables

Chapter 1

Introduction

1.1. Motivation and Objective

The design of efficient digital communication systems is a challenge which is influenced by a number of factors such as the available technology, the type of service aimed for (e.g. speech, data, facsimile, video, images, etc.), the acceptable cost of the system, the channel characteristics, new ideas in research, and regulations. The driving force behind this challenge today for future digital communication systems is the demand for higher data rates and systems capable of supporting many different types of services with different bit error probability and delay requirements.

To this end Multicarrier modulation (MCM) [1] is one of the best candidates and is fast becoming the de facto standard for present and future high speed communication systems. Multicarrier modulation (also called orthogonal frequency division multiplexing OFDM) is a technique of dividing digital data to be transmitted as several interleaved bit streams, and using these to modulate a number of subcarriers. It is the basis for WLAN standards IEEE 802.11a/g [2] and HIPERLAN/2 [3], WMAN standard IEEE 802.16 [4], broadcasting standards DAB (Digital Audio Broadcasting) [5] and DVB (Digital Video Broadcasting) [6], and digital subscriber line standards ADSL and VDSL. It is also being considered for the future ultrawideband communication systems.

In OFDM, subchannels are obtained with an orthogonal transformation using discrete Fourier Transform (DFT) [7] on each block of data. The DFT exhibits the desired orthogonality and can be implemented efficiently through the fast Fourier transform (FFT) algorithm.

Orthogonal transformations are used so that at the receiver, the inverse transformation can be used to demodulate the data without error in the absence of noise. Efficient modulation and coding schemes can be used in the individual subchannels to approach the capacity of the channel. OFDM schemes use rectangular pulses for data modulation; hence a given subchannel has significant spectral overlap with a large number of adjacent subchannels. Hence subchannel isolation is retained only for channels which introduce virtually no distortion. But typical channels are far from ideal, and introduce interference that reduces system performance.

One of the key ideas behind the MCM realization is the use of guard interval that contains a cyclic prefix, which is used to overcome intersymbol interference (*ISI*) caused by the delay spread of the channel [8,9] and make equalization at the receiver a simple scalar multiplication (frequency domain equalization). However this performance comes at the cost of i) a loss of spectral efficiency and ii) poor spectral concentration of the subcarriers.

An alternative approach to MCM is based on discrete wavelet transform (DWT), which leads to highly structured and thus efficiently realizable transmission signal sets. Wavelet-based OFDM has gained popularity in the literature recently. Due to very high spectral containment properties of wavelet filters, wavelet OFDM can better combat narrowband interference and is inherently more robust with respect to intercarrier interference (*ICI*) than traditional FFT filters. Since there is no cyclic prefix present in wavelet implementation the data rates can surpass those of FFT implementations.

1.1.1 Objective of the thesis work

The objective of this paper is to carryout a simulation of the DFT and DWT based MCM systems and analyze their performance under AWGN and multipath fading channels. An appropriate channel model will be implemented and the communication link performance for both MCM schemes will be studied and presented.

The **specific objectives** are:

- Establish an appropriate channel and system model for wavelet based MCM
- Perform simulation based performance analysis of wavelet based MCM in comparison with DFT-based OFDM under different scenario.

1.2. Previous Related Research

The principle of transmitting data in parallel using multiple carriers on the same channel dates back more than 40 years. The first systems using MCM were military high frequency (HF) radio links in the late 1950s and early 1960s. One of these systems is the Kineplex [61], single side band (SSB) high frequency (HF) frequency division multiplex (FDM) system with closely spaced tones operating at 3kbps. The paper describing the Kineplex system also shows its bit error rate vs. signal to noise ratio performance with frequency shift keying (FSK) modulation.

Another similar MCM system is the Kathryn modem [62], which transmits large number of subcarriers, each BPSK modulated, in SSB mode. The following year Zimmerman et al presented the Kathryn modem with all its capabilities including variable transmission rate, channel coding and the frequency multiplexing is done by Fourier transform using analog signal processing [63]. In 1968 Chang presented a theoretical analysis of the performance of an orthogonal multiplexing data transmission scheme subject to a number of degrading factors like sampling error, phase error and developed a simple formula for computing *ICI* and *ISI* [64].

OFDM is a special form of MCM with densely spaced sub-carriers and overlapping spectra, whose main idea was patented by Chang, from the Bell Labs, in 1966, but it was only after the paper done by Bingham [1] that it got its popularity now. The earliest prominent work on system description and the performance analysis of multicarrier systems is done by Saltzberg [10]. The system described use infinitely long symbols that are strictly band-limited with

orthogonal subcarriers overlapping in frequency. He concluded by pointing out that the design trend in multicarrier systems should be towards reducing crosstalk between adjacent channels rather than on perfecting the individual channels. A major paper by Weinstein and Ebert [7] described the use of DFT for generating overlapping orthogonal subcarriers implemented using efficient processing and eliminating the bank of subcarrier oscillators. They also used raised cosine window function in time domain and guard interval between symbols for combating *ISI* and *ICI*. Cimini also did analysis and simulation of DFT based OFDM system using pilot-based correction for combating the effects of multipath propagation and *ICI* on narrow-band digital mobile channel [9].

Steendam and Moeneclaey investigated the effect of the number of subcarriers and the guard time duration on the performance of OFDM systems operating on a frequency-selective time-selective channel [11]. Intern Kim *et al* analyzed the combined influence of *ISI* and *ICI* on the performance of Reed-Solomon (RS) coded OFDM system [12]. They went on observing that there is an optimum number of subcarriers that minimizes the decoding error probability of the RS code for each channel state.

Amara Graps presented a paper introducing wavelets. He gave an historical perspective in transforms and also the comparative analysis of Fourier transform and wavelet transforms [50]. Wornell worked on multirate signal processing and wavelets presenting the emerging applications of wavelets in digital communication [65]. The theoretical work and also the design of wavelet in connection with filter bank by Vetterli[66].

Heather Newlin presented a paper on the ongoing developments of the use of wavelets in the field of communication [56]. Sandberg and Tzannes [13] presented an alternative digital baseband MCM system which they called overlapped discrete multitone or discrete wavelet multitone (DWMT). The system they described is based on the application of M-band wavelet filters and the pulses for different data blocks overlap in time. The design of the pulses shows spectral containment and bandwidth efficiency and performance on different network structures better than DFT based MCM systems.

At the 5th international OFDM-workshop Kozek *et al* [14] presented a comparison of wavelet-type, Gabor-type (OFDM and DMT) and also Wilson-type (offset-QAM/OFDM) transmultiplexer structures. Using linear distortion (perturbation) caused by time-invariant channels as performance measure they concluded that Gabor structures show optimum perturbation stability. Similarly, Zhang *et al* presented their findings of comparison, on DFT-OFDM and DWT-OFDM on three different channel models and showed that generally DWT-OFDM BER performance is better than DFT-OFDM [15].

1.3. Organization of the Thesis Work

The outline of this thesis will be as follows:

Chapter 2 Channel Characterization

The radio channel model is probably the most important tool for the design of communication systems. It has to appropriately describe the relevant properties of the physical channel, and it should be suitable for analytical studies and computer simulations. As such chapter 2 gives a description of the channel model encountered by the MCM system used in the performance analysis study.

Chapter 3 Multicarrier Modulation Transmission

Here introduction and overview to the MCM transmission system will be presented. System models will be described for analyzing the performance of OFDM. And also a treatment of the challenges of MCM in the form of PAPR, sensitivities to synchronization errors is done. The chapter also gives the account of why MCM is selected against single carrier methods.

Chapter 4 Discrete Wavelet Transform

Chapter 4 presents a discussion of the basic wavelet theory, the continuous wavelet transform (CWT) and discrete wavelet transform (DWT). Then, DWT based OFDM system will be described.

Chapter 5 Simulations and Results

In this chapter, first the description of the simulation set up for the MCM system study, then the results of this simulation study with a discussion of the results will be presented.

Chapter 6 Conclusion and Future Work

This chapter concludes by summarizing the results of the thesis work and their particular significances. Areas for future work will also be suggested.

Chapter 2

Channel Characterization

Radio-wave propagation through wireless channels is characterized by randomly time varying effects such as path loss, frequency selective fading, Doppler spread and multipath delay-spread. These channel effects produce loss on the received average signal power which is termed as fading, broadening of the signal pulses causing the pulses smear into each other bringing about what is known as intersymbol interference (*ISI*) and also and also a shift on the signal phase which may introduce a loss of orthogonality between carriers causing intercarrier interference (*ICI*). Thus, the importance of proper channel modeling for designing and analyzing radio interfaces for wireless communications systems cannot be stressed enough. The goal of this chapter is the description and discussion of an appropriate channel model for such systems.

2.1. Noise

Noise in communication systems generally refers to the unwanted random process that introduces distortion to the transmission and processing of the signal of interest. Its presence is inevitable and it is a limiting factor on the power required in the transmission of the information-bearing signal over the channel.

Noise is random in nature and is usually independent of the signal of interest. It may originate from the surrounding environment, components in the communication system, such as nonlinear amplifiers and quantizers, and other electrical devices at the receiver can also introduce noise. Therefore, the noise from different sources is lumped together, and the net effect is modeled as an additive component to the received signal and it is commonly referred to as channel noise or receiver front end noise.

Noise introduced at the receiver input belongs to the class of thermal noise. It is often statistically characterized as a random gaussian process with zero-mean, and uncorrelated with the transmitted data.

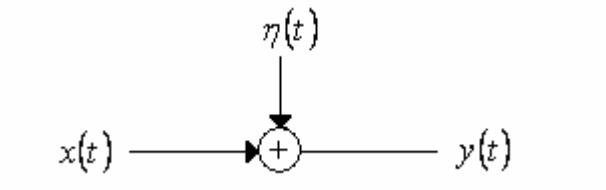

$$y(t) = x(t) + \eta(t)$$

Figure 2.1 Channel noise Model

Here $\eta(t)$ is complex-valued baseband representation of the noise. In order to simplify the analysis of the system performance, the channel noise is assumed white with power spectral density of $\frac{N_0}{2}\frac{W}{Hz}$ [22]. Hence the name *additive white gaussian noise* (*AWGN*).

2.2. Multipath Fading Channel

During propagation, radio signals loose strength with distance. This is due to the wave front of the radio signal expanding and thus reducing in power density. As such path loss and shadowing in radio channel are described by *large-scale* channel models [16-20], which essentially provide information about the average received power at a certain location. *Path loss* describes the dependency of this average power on the distance between transmitter and receiver, while *shadowing* accounts for the fluctuations observed at a fixed distance, due to geometric features of the propagation environment. The statistics of large-scale fading provide a way of computing an estimate of path loss as a function of distance which is described in terms of a mean-path loss and log-normally distributed about the mean.

Due to reflections, refractions, and scattering of the radio wave by structures in the medium, the transmitted signal reaches the receiver via more than one path, resulting in phenomenon referred to as *multipath propagation*. In narrowband transmission the multipath channel causes fluctuations in the received signal envelope and phase. In wideband pulse transmission, on the other hand, the effect is to produce a series of delayed and attenuated pulses for each

transmitted pulse, giving rise to *multipath fading* and interference. The effects of multipath propagation are usually modeled by *small-scale* variations [16-20]. Small-scale models are valid within (small) local areas, where the signal fluctuations due to shadowing and path loss can be neglected.

2.3. Mathematical Modeling of the Channel

2.3.1. Channel Impulse Response (*CIR*)

The received signal at the output of a wireless channel is a superposition of multiple signals arriving along different paths. Each of these paths generally have different delays and attenuation. The *channel impulse response* is thus the sum of discrete multipath components impinging on the receiver. In complex lowpass equivalent notation, *CIR* can be written as:

$$h(\tau,t) = \sum_k \alpha_k(t) e^{-j\theta_k(t)} \delta[\tau - \tau_k(t)] \qquad (2.1)$$

where t and τ are the observation and application times of the impulse, respectively. $\alpha_k(t)$, $\tau_k(t)$, $\theta_k(t)$ are time-varying attenuation factor, propagation delay (arrival time), and phase shift of the k^{th} propagation path, respectively [22]. The channel is completely characterized by these path variables [21]. The *CIR* is usually characterized as wide-sense-stationary complex-valued random process, and in most cases the attenuation, phase shift and propagation delay associated with each propagation path are assumed uncorrelated. Thus the channel is modeled as *wide-sense-stationary uncorrelated scattering* (*WSSUS*) [22], [23].

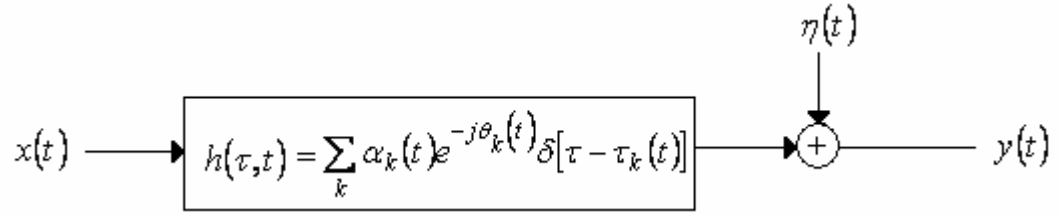

$$y(t) = \int_{-\infty}^{\infty} x(\tau) h(\tau,t)\, d\tau + \eta(t)$$

Figure 2.2 Mathematical Model of multipath fading channel.

2.3.2. Channel Transfer function

The time-dispersive channel can also be equivalently described in frequency domain by taking the Fourier transform of the CIR

$$H(f,t) = \int_{-\infty}^{\infty} h(\tau;t) e^{-j2\pi f\tau} d\tau = \sum_n \alpha_n e^{-[j2\pi f\tau_n + \theta_n]} \qquad (2.2)$$

which gives the *channel transfer function* having the same statistics as $h(\tau;t)$[22],[23].

2.3.3. Channel Correlation functions

The dispersive effects of the multipath channel are best understood by examining the autocorrelation of the channel response $h(\tau,t)$. With the assumption that $h(\tau,t)$ is a wide-sense- stationary complex random process and that the scatterers in the multipath propagation are uncorrelated at different delays τ_1 and τ_2, the autocorrelation function depends only on the time difference $\Delta t = t_1 - t_2$ and is given by

$$R_h(\tau_1,\tau_2;t_1,t_2) = \frac{1}{2} E\left[h^*(\tau_1,t) h(\tau_2,t+\Delta t)\right] = R_h(\tau;\Delta t)\delta(\tau_1-\tau_2) \qquad (2.3)$$

where *E*[ ] is the expectation operator.

By letting Δt = 0, the *multipath intensity profile* or *delay power spectrum* of the channel $R_h(\tau)$ is obtained [18],[20],[23]. This quantity is the average power at the channel output as a function of the delay τ.

The duration of relative delay time over which multipath components of the transmitted signal arrive with a signal power at certain level considered to be nonzero is called the *multipath delay spread* of the channel or the *maximum excess delay* and is defined as τ_m. The delay spread tends to increase with the propagation path length and antenna heights. Thus, it is significantly larger for outdoor systems than for indoor wireless transmission. If the maximum excess delay τ_m, exceeds the symbol duration T_{sym}, then the energy of a transmitted symbol will be dispersed into other signaling intervals causing *ISI*.

An equivalent channel correlation function using the channel transfer function $H(f,t)$ is the spaced-frequency, spaced-time correlation function expressed as

$$R_H(\Delta f,\Delta t) = \frac{1}{2}E\left[H^*(f,t)H(f+\Delta f,t+\Delta t)\right] \tag{2.4}$$

where $\Delta f = f_1 - f_2$. Here also setting $\Delta t = 0$ in equation 2.4, it can be shown that at $R_H(\Delta f)$ and $R_h(\tau)$ are Fourier transform pairs [19]:

$$R_H(\Delta f) = \int_{-\infty}^{\infty} R_h(\tau)e^{-j2\pi\Delta f\tau}d\tau \tag{2.5}$$

The spaced-frequency correlation function $R_H(\Delta f)$ is a function in frequency domain, and thus provides us with a measure of the frequency coherence of the channel [22]. In relation to $R_H(\Delta f)$, the range of frequencies over which spectral components of the transmitted signal pass through the channel and arrive at the receiver with essentially equal gain and linear phase is termed as the *coherence bandwidth*, B_c, of the channel. The coherence bandwidth and the delay spread are reciprocally related ($B_c \approx \frac{1}{\tau_m}$), but an exact relation between them does not exist, and must be derived from signal analysis of actual signal dispersion measurements in a particular channel.

2.3.4. Doppler Spread

The time variation in the channel measured by the parameter Δt in $R_H(\Delta f,\Delta t)$, which arise from the transmitter or receiver motion, causes the *Doppler spreading* and *Doppler shift* of the received signal spectral line. By setting $\Delta f = 0$, the function $R_H(\Delta t)$, termed as the spaced-time correlation function, specifies the extent to which there is correlation between the channels response to signals sent at times t_1 and t_2.

$$R_H(\Delta t) = \frac{1}{2}E\left[H^*(f,t)H(f,t+\Delta t)\right] \tag{2.6}$$

The duration of time over which the channel response is expected to be invariant is called the channel *coherence time*, T_c [19]. The coherence time T_c together with the channel spaced-time correlation function $R_H(\Delta t)$ give us the information as to how fast signal fading occurs within the channel.

The Doppler effect can be characterized by taking the Fourier transform of $R_H(\Delta t)$ relative to Δt :

$$S(f) = \int_{-\infty}^{\infty} R_H(\Delta t) e^{-j2\pi f \Delta t} d\Delta t \qquad (2.7)$$

The expression $S(f)$ is a function of the Doppler frequency called the *Doppler power spectrum* of the channel which indicates the level of signal intensity [17],[18],[22].

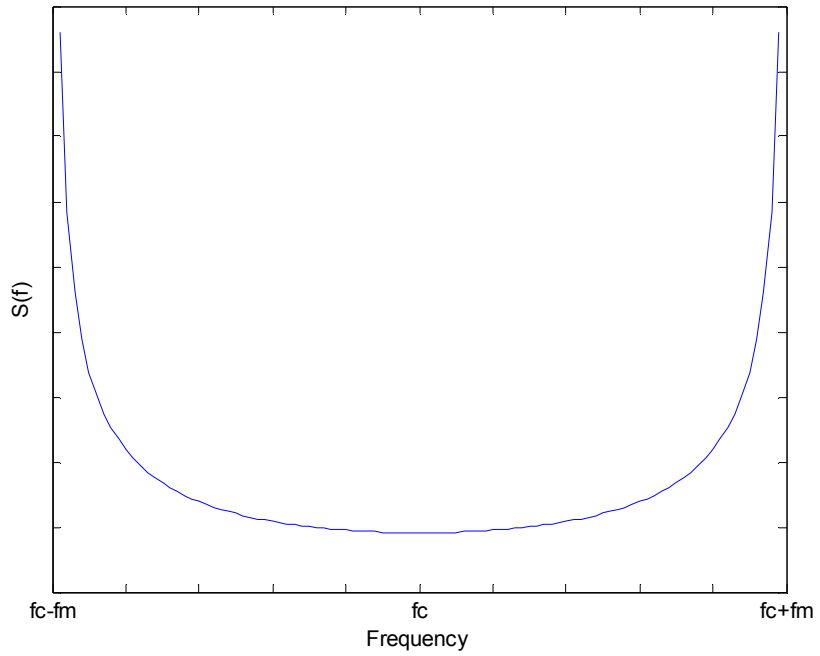

Figure 2.3 A plot of simulated Doppler spectrum.

The range of values of Doppler frequency f over which the received signal intensity is essentially nonzero is called channel *Doppler spread*, denoted f_D ($T_c \approx \frac{1}{f_D}$).

2.3.5. Multipath Fading Types

Flat and Frequency Selective Fading

Frequency selectivity characteristics of a multipath fading channel is determined in time-domain by the relationship between the channel's maximum excess delay τ_m and symbol duration T_{sym}, and in frequency domain between the channel's coherence bandwidth B_c and the bandwidth of the transmitted signal *W*. A channel exhibits *frequency selective fading* if $\tau_m > T_{sym}$ (or $B_c < W$), that is the received multipath component of a symbol extend beyond the symbols time duration or equivalently when the spectral components of a signal are not all affected equally by the channel. Such multipath dispersion of the signal results in *ISI* [17-19],[22].

On the other hand, if $\tau_m < T_{sym}$ (or $B_c > W$), all the received multipath components of a symbol arrive within the symbol time duration. Here, all the signal's spectral components will be affected similarly by the channel and hence the channel is said to be *frequency non-selective* or *flat fading*. Flat fading does not introduce *ISI* distortion, but performance degradation occurs due to loss of *SNR* whenever there is signal fading.

Slow and Fast fading channel

The distinction between *fast fading* and *slow fading*, which is due to the time-variant nature of the channel, is also important for the mathematical modeling of fading channels and for the performance evaluation of communication systems operating over these channels. This notion is related to the coherence time T_c of the channel and symbol duration of the transmitted signal.

The fading is said to be slow if the symbol time duration T_{sym} is smaller than the channel's coherence time T_c, that is, the channel changes much slowly than symbol duration. Thus, the channel state remains unchanged during the time over which a symbol is transmitted. This does not imply that the effects of the channel can be neglected, there will be degradation due

to loss of *SNR*, but it is possible to track the changes in the channel to appropriately compensate for the channel dynamics.

Fast fading, $T_c < T_{sym}$, occurs when the channel fading characteristics varies rapidly. This causes frequency dispersion due to Doppler spreading, which leads to baseband signal pulse shape distortion. This baseband pulse shape distortion due to fast fading brings about a loss in *SNR* resulting in an irreducible error rate. Such distorted pulses cause synchronization problems and difficulties in adequately defining the matched filter [19].

2.4. Rayleigh Fading Model

Multipath fading is due to the constructive and destructive combination of randomly delayed, reflected, scattered and diffracted signal components. This type of fading is relatively fast and is therefore responsible for the short term signal variations. Depending on the nature of the radio propagation environment, there are different models describing the statistical behavior of the multipath fading envelope.

A well accepted and frequently used model for multipath fading in the absence of a strong received component or with no direct line-of- sight (LOS) path is the Rayleigh distribution with probability density function (pdf) of the k^{th} path fading amplitude α_k is given by [21]

$$f(\alpha_k) = \frac{\alpha_k}{\sigma^2} \exp\left(-\frac{\alpha_k}{2\sigma^2} \right), \qquad \alpha_k \geq 0 \tag{2.8}$$

where α_k are path amplitudes and σ is the Rayleigh parameter with $\sqrt{\frac{\pi}{2}}\sigma$ being the mean and $(2-\frac{\pi}{2})\sigma^2$ the variance.

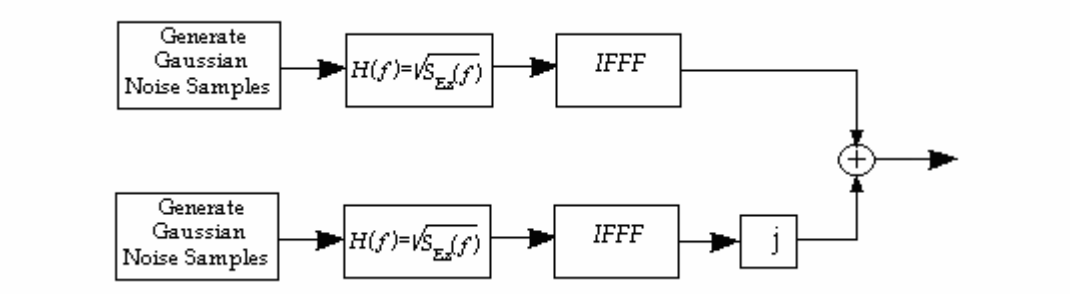

Figure 2.4 Clark's Rayleigh Fading Model

Here, the model (Clark's model [16]) assumes that the transmitted signal reaches the receiver via N directions. The k^{th} path having a complex strength of $\alpha_k e^{-j\theta_k}$ is described by the envelope α_k and phase θ_k. In the absence of a strong component, the resultant phasor at the receiver will be

$$\alpha e^{-j\theta} = \alpha' \sum_k e^{-j\theta} \tag{2.9}$$

The envelope α and phase θ are independent, α being Rayleigh distributed and θ having a uniform $[0, 2\pi)$distribution. This is a consequence of the path phase being very sensitive to the path length, changing by 2π as the path length changes by a wavelength. Also the quadrature components *I* and *Q* of the received signal, which are the sum of a large number of sinusoids with approximately constant amplitude and uniform phases, are independent and, by the central limit theorem, gaussian distributed random variables. This results in Rayleigh distributed envelop α [24].

2.5. Multipath Channel Model for OFDM

For the k^{th} subcarrier frequency the multipath channel impulse response is expressed as

$$h_k(\tau) = \sum_{i=1}^{M} \left\{ \alpha_i e^{(-j2\pi f_k \tau_i)} \delta[\tau - \tau_i] \right\} \tag{2.10}$$

where M is the total number of multipath components. When delay spread is within the guard interval, because of the action of the cyclic prefix no *ISI* and *ICI* will occur when demodulating the signal x_k. The demodulated signal y_k is therefore given by

$$y_k = x_k \sum_{i=1}^{M_0} \alpha_i e^{(-j2\pi f_k \tau_i)} \tag{2.11}$$

where M_0 is the number of paths having delays within the guard interval.

The reception of multipath components in which the delay doesn't exceed the guard interval is equivalent to the reception of a single-path component without delay spreading. Thus, the equivalent impulse response is given by

$$h_k(\tau) = \sum_{i=1}^{M_0} \left\{ \alpha_i e^{(-j2\pi f_k \tau_i)} \right\} \delta[\tau] \tag{2.12}$$

When delay spread exceeds the guard interval, the impulse response is equivalent to the incidence of OFDM signal without guard interval having a delay of $\tau_i - T_{GI}$, thus

$$h_k(\tau) = \sum_{i=M_0+1}^{M} \left\{ \alpha_i e^{(-j2\pi f_k \tau_i)} \delta[\tau - \tau_i + T_{GI}] \right\} \tag{2.13}$$

where T_{GI} is the guard interval.

Chapter 3

Multicarrier Modulation Transmission

The key idea of multicarrier modulation (MCM) is to partition a high-rate data stream into a large number of low rate data streams and transmit them over equidistantly spaced subchannels. As the occupied bandwidth of a signal is in principle reciprocal to its symbol rate, the sum of all low-rate data streams occupies the same bandwidth as the high-rate signal. The low-rate signals are much less susceptible to channel impairments and thus reconstruction of the subchannel signals at the receiver side is simplified to a great extent. However, all subchannel signals are transmitted in parallel and thus have to be processed simultaneously at the receiver. The most widely used multicarrier transmission systems are the wireless based OFDM and the wireline Discrete Multi-Tone (DMT) [1] [7] [9] [13] [18]. This chapter presents the description of OFDM system.

3.1 Orthogonal Frequency Division Multiplexing

Orthogonal frequency division multiplexing (OFDM) scheme is based on the multicarrier communications technique. In OFDM the spectra of subcarriers overlap each other but the frequency spacing between them is selected such that the subcarriers are mathematically orthogonal to each other.

Figure 3.1 shows a block diagram of a basic OFDM system. Discrete Fourier Transform (DFT) efficiently implemented by Fast Fourier Transform (FFT) is used to modulate and demodulate the data constellations on the orthogonal subcarriers [7]. This baseband signal processing algorithms effectively replace the bank of I/Q modulators and demodulators that would otherwise be required.

To generate a baseband OFDM symbol, a serial digitized data stream is first channel coded and then modulated using phase shift keying (PSK) or quadrature amplitude modulation (QAM). These data symbols are converted from serial-to-parallel into N data constellation points before modulating the subcarriers using IFFT, where N is the number of IFFT points.

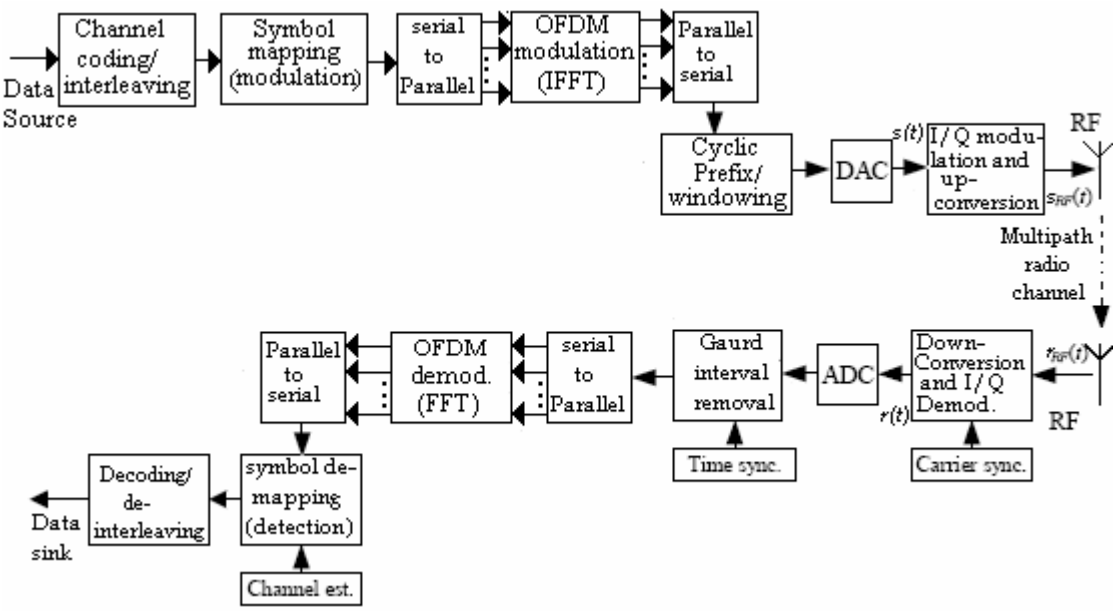

Figure 3.1 Basic Block diagram of OFDM system

The time domain OFDM modulated symbol output of the IFFT is converted back to a serial stream and a guard interval in the form of cyclic prefix is added to each OFDM symbol. The basic pulse shape for the symbols is rectangular which have large bandwidth due to its sinc-shaped spectrum. Thus windowing is necessary to reduce the out of band energy of the sidelobes. Then the symbol stream is converted to analog form for passband processing and transmission.

The receiver performs the exact opposite of the transmitter. After passband processing at the RF Front-end, the baseband processing will be performed. This includes guard interval removal and serial-to-parallel conversion before the DFT demodulation. Furthermore, synchronization and channel estimation are done for interference free subcarrier demodulation using FFT and also constellation decoding.

3.2 OFDM System Model

OFDM divides the available spectrum into several narrowband overlapping and orthogonal subchannels. These narrowband channels experience almost flat fading, which makes receiver processing relatively simple. There are several versions of OFDM system [1] [7] [25], but cyclic prefixed based OFDM is selected for this study.

The system model described here uses a simplified model with the following assumptions: OFDM symbol duration with cyclic prefix is $T = T_{cp} + T_{sym}$, where T_{sym} is the effective symbol duration and cyclic prefix (CP) of length T_{cp}. The frequency separation between adjacent sub-carriers is equal to the inverse of the effective symbol interval T_{sym}, which is the minimum frequency separation required to achieve orthogonality between two complex sub-carriers. A total of N subcarriers are used with total bandwidth of $W = N/T_{\text{sym}}$ Hz. The transmitter and receiver are assumed perfectly synchronized and the fading is slow enough for the channel to be considered constant during one OFDM symbol.

3.2.1 Continuous-time system model

The first MCM systems design did not make use of digital modulation and demodulation. The continuous-time OFDM model illustrated in Figure 3.2 below is considered for convenience, which in practice is digitally synthesized [26].

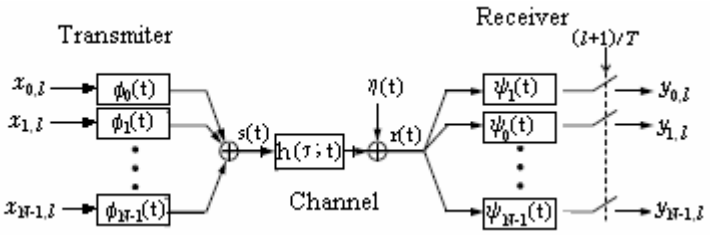

Figure 3.2 Simplified continuous-time baseband OFDM model

The Transmitter

In this model, the transmitter uses rectangular pulse for transmission purposes which are expressed as

$$\phi_k(t) = \begin{cases} \frac{1}{\sqrt{T_{sym}}} e^{j\frac{2\pi kt}{T_{sym}}} & -T_{cp} < t < T_{sym} \\ 0 & otherwise \end{cases} \quad (3.1)$$

The baseband transmitted signal for OFDM symbol l on the baseband carrier frequency $f_k = k/T_{sym}$, is expressed as

$$S_l(t) = \sum_{k=0}^{N-1} x_{k,l}\phi_k(t - lT) \quad (3.2)$$

where $x_{k,l}$ are complex numbers representing a set of signal constellation points. When an infinite sequence of OFDM symbols is transmitted, the output of the transmitter is a juxtaposition of individual OFDM symbols

$$s(t) = \sum_{l=-\infty}^{\infty} S_l(t) = \sum_{l=-\infty}^{\infty} \sum_{k=0}^{N-1} x_{k,l}\phi_k(t - lT) \quad (3.3)$$

The Channel

The influence of the time-dispersive, multipath fading radio channel is expressed by its lowpass equivalent $CIR, h(t;\tau)$. Then with the assumption that the channel delay spread is within $[0, T_{CP}]$, the received signal $r(t)$ after the cyclic prefix is removed will be

$$r(t) = \int_0^{T_{cp}} h(t;\tau)s(t - \tau)d\tau + \eta(t) \quad (3.4)$$

where $\eta(t)$ is additive white complex gaussian channel noise, with zero mean and double sided power spectral density of $N_0/2$.

The Receiver

The OFDM receiver uses bank of filters matched to the transmitter waveforms given by

$$\Psi(t) = \begin{cases} \phi_k^*(T - t) & if\ t \in [0, T - T_{cp}] \\ 0 & otherwise \end{cases} \quad (3.5)$$

And the sampled output of the m^{th} receiver filters which are matched to the effective part of the symbol $[T_{cp}, T]$, is given by

$$y_m = \frac{1}{\sqrt{T_{sym}}} \int_{T_{cp}}^{T} r(t) e^{-j\frac{2\pi kt}{T_{sym}}} dt \tag{3.6}$$

$$= \frac{1}{T_{sym}} \sum_{0}^{N-1} x_m h_m \int_{T_{cp}}^{T} e^{j\frac{2\pi mt}{T_{sym}}} e^{-j\frac{2\pi kt}{T_{sym}}} dt + \eta_m$$

where h_m expressed as

$$h_m = \int_{T_{CP}}^{T} h(\tau) e^{-j\frac{2\pi m\tau}{T_{sym}}} d\tau \tag{3.7}$$

is the sampled frequency response of the channel at the m^{th} subcarrier frequency, and $\eta_m = \int_{T_{CP}}^{T} \eta(T-t)\phi_k^*(t)dt$ is the additive white gaussian noise (AWGN). Since the transmitter waveforms $\phi_k(t)$'s are orthogonal,

$$\int_{T_{CP}}^{T} \phi_k(t)\phi_m^*(t)dt = \frac{1}{T_{sym}} \int_{T_{CP}}^{T} e^{j\frac{2\pi mt}{T_{sym}}} e^{-j\frac{2\pi kt}{T_{sym}}} dt = \delta[k-m]$$

where $\delta[k]$ is the Kronecker delta function [27], and thus equation (3.6) can be simplified to

$$y_k = x_k h_k + \eta_k \tag{3.8}$$

The rectangular transmitter pulse shapes result in a sinc-shaped frequency response for each channel as shown in Figure 3.3 below. The sidelobes for the sinc function decay as $1/f^2$ which is not efficient and thus windowing is required to reduce the sidelobe energy.

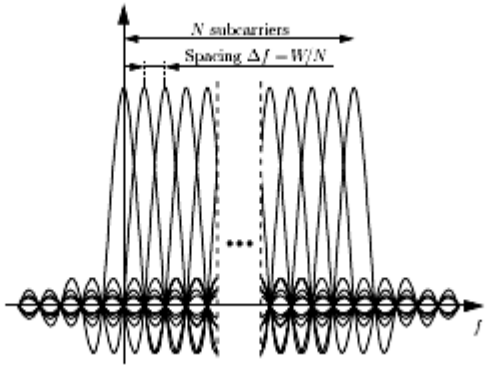

Figure 3.3 Subcarrier spectrum of OFDM system

3.2.2 Discrete-time system model

In the discrete-time model of an OFDM system, the modulation and demodulation are performed by an *inverse* DFT and DFT respectively [7]. The cyclic prefix is added in the same way and the channel operation is discrete-time convolution.

The discrete transmitted signal is obtained by sampling the continuous time signal expressed in (3.3) at time intervals $t_n = nT_s$, where $T_s = T_{sym}/N$. The normalized discrete transmitted signal with cyclic prefix of length $N_{cp} = T_{cp}/T_s$ is given as [22],[26]

$$s(n) = \frac{1}{\sqrt{N}} \sum_{k=0}^{N-1} x_k e^{j\frac{2\pi kn}{N}} \qquad n \in [-N_{cp}, N-1] \tag{3.9}$$

Equation (3.9) is an N-point inverse DFT of a discrete data sequence $x[k]$, $0 \le k \le N-1$, which can be efficiently implemented using IFFT algorithm.

Since the signal bandwidth is limited to W, the WSSUS channel can also be modeled as a tapped delay line with random taps. Here also with the same assumption that $N_{cp} \ge L$ the total delay of the channel coefficients $h(n,l)$, the discrete received signal after the cyclic prefix is removed is given by

$$r(n) = \sum_{l=0}^{L} h(n,l)S(n-l) + \eta(n) \qquad n \in [0, N-1] \tag{3.10}$$

where $\eta(n)$ is complex gaussian random variable with zero mean and variance $N_0/2$ per dimension. Then, to demodulate the symbols on different subcarriers, we perform FFT on $r(n)$, and obtain

$$y_k = x_k h_k + \eta_k \tag{3.11}$$

η_k is white gaussian noise. If the channel coefficients h_k are equal, that is the channel is time invariant over one OFDM symbol period, there will be no *ICI*.

3.3 Guard time and Cyclic Prefix

By transmitting information on N sub-carriers, the symbol duration of an OFDM signal is N-times longer than the symbol duration of an equivalent single-carrier signal. Accordingly, *ISI* effects introduced by linear time dispersive channels are minimized. However to effectively eliminate the effects of *ISI* a guard time is inserted with duration longer than the expected duration of the impulse response of the channel [7] [28]. Moreover, to eliminate *ICI* the guard time is cyclically extended. The cyclic prefix is thus the last T_{cp} samples of the OFDM symbol prepended to the beginning of the symbol as shown in figure 2.2. At the receiver, the first T_{cp} samples of the OFDM symbol are discarded.

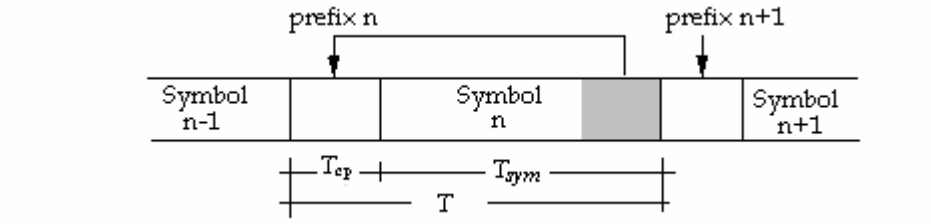

Figure 3.4 The Cyclic Prefix

The cyclic prefix added to the OFDM symbol converts the linear convolution action of the channel into a circular convolution. Such a cyclic convolution after DFT in the receiver reduces equalization to a simple multiplication. In typical OFDM systems the cyclic prefix amounts to 5% to 30% of the total symbol length, depending on symbol duration and the expected channel impulse response [29].

3.4 Windowing

For a finite number of sub-channels, the OFDM spectrum exhibits a relatively slow decay, according to a sinc function. Such a spectral characteristic will therefore cause high interference to users of adjacent frequency bands. Windowing is a technique used to reduce these sidelobes and thereby reduce the signal power transmitted out of band and to allow the amplitude of an OFDM symbol to go smoothly to zero at the symbol boundaries [31]. A commonly used window type is the raised cosine window with rolloff factor β, defined as

$$w(t)=\begin{cases}0.5+0.5\sin(\pi+t\pi/2T) & t\in[0,\beta T]\\ 1.0 & t\in[\beta T,T]\\ 0.5+0.5\cos(\pi(t-T)/\beta T) & t\in[T,(1+\beta)T]\end{cases} \tag{3.12}$$

In an OFDM system, the applied window must not influence the signal during its effective period. Accordingly, the cyclic extended parts of the signal are pulse-shaped as depicted in Figure 3.5. The rolloff factor β reduces the guard interval by βT_s.

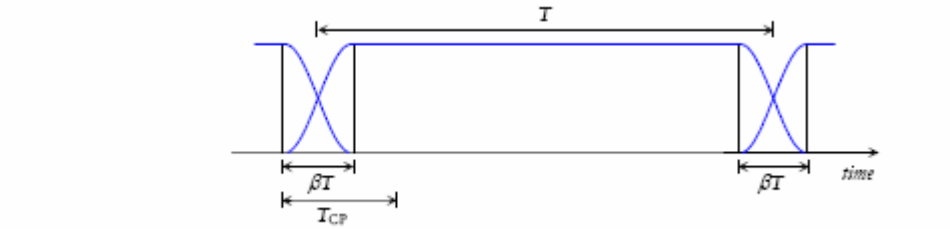

Figure 3.5 Cyclic Prefix and Windowing of OFDM symbol

The OFDM symbol incorporating windowing is now expressed as

$$s(t)=2\,\mathrm{Re}\left\{w(t)\sum_{k=0}^{N-1}x_k e^{j\frac{2\pi kt}{T}}\right\} \qquad t\in[0,T] \tag{3.13}$$

3.5 Intersymbol and Intercarrier Interference

In a multipath environment, a transmitted symbol takes different times to travel through different propagation paths. Thus, the multipath channel creates time dispersion in which the duration of the received symbol is extended. Extending the symbol duration causes the current received symbol to overlap with the previously received symbols and results in intersymbol interference (*ISI*). In OFDM, *ISI* usually refers to interference of an OFDM symbol with a previous symbol.

The spectra of subcarriers, in OFDM, overlap but remain orthogonal to each other. This means that at the maximum of each subcarrier spectrum, all the spectra of other subcarriers are zero. When orthogonality is lost, data symbols on adjacent subcarriers will interfere which is referred to as intercarrier interference (*ICI*).

The demodulated symbol $y_{k,l}$, as in Equation (3.6), at the subcarrier k/T_{sym} during the l-th OFDM symbol, on the integration interval $t \in [kT, kT+T_{sym}]$, can be expressed as

$$y_{k,l} = \frac{1}{\sqrt{T_{sym}}} \left(\int_{lT}^{lT+T_{sym}} r_l(t) e^{-j\frac{2\pi k(t-kT)}{T_{sym}}} dt + \sum_{l'=-\infty, l' \neq l}^{\infty} \int_{lT}^{lT+T_{sym}} r_{l'}(t) e^{-j\frac{2\pi k(t-kT)}{T_{sym}}} dt \right) \quad (3.14)$$

where the first term consists of the useful symbol with *ICI* and the second term is the *ISI*.

If the guard interval is of sufficient length, localizing the channel response within the cyclic prefix, then Equation (3.14) reduces to $y_{k,l} = x_{k,l} h_{k,l} + \eta_{k,l}$ as expressed in Equation (3.8). In this case, the transmitted symbol is completely recovered by multiplying the demodulated symbol by the channel coefficients $h^{-1}{}_{k,l}$, if the channel is perfectly known at the receiver.

The interference power for both *ISI* and *ICI* is derived for time-invariant channel in [32]. They used a channel model truncated to that within the cyclic prefix and outside it. They have found that the interference power is dependent on multipath channel profile outside the cyclic prefix, the system parameters T_{cp}, T_{sym} and the symbol energy Es. Also if τ_{max} - T_{cp}, τ_{max} maximum delay spread of the channel, is relatively small compared with the OFDM symbol duration, then the *ICI* power is approximately equal to the *ISI* power given as,

$$P_{ISI} = \frac{E_s}{T_{sym}} \int_{t=0}^{\tau_{\max}-T_{cp}} \int_{\tau=t+T_{cp}}^{\tau_{\max}} R(\tau) d\tau dt \quad (3.15)$$

where $R(\tau)$ is the channel intensity profile described in section 2.3.3.

3.5.1 Effects of Number of Subcarriers and Cyclic Prefix Duration

In a multipath channel, if the cyclic prefix is longer than the delay spread no interference will result since the channel effects can be easily compensated by an equalizer. The distortion caused by *ISI*, however, gets bigger as the delay spread exceeds the duration of the cyclic prefix more, resulting in high *BER*.

The influence of *ISI* in multipath channel can be reduced by increasing the duration of an OFDM symbol. For a given bandwidth of an OFDM signal, the symbol duration is proportional to the number of subcarriers. If delay spread of the channel is large, a significant number of samples of individual OFDM symbols are affected by *ISI* and thus the system will have a high *BER*. On the other hand, if the delay spread is small, a small portion of the individual OFDM symbols is affected by *ISI* and thus the system will have a low *BER*.

OFDM symbols with long duration are more resilient to frequency-selective fading but more sensitive Doppler spread. Doppler spread results in loss of orthogonality between subcarriers. For a given signal bandwidth, the frequency spacing between subcarriers decreases as the number of subcarriers increases. The small frequency separation between the subcarriers makes them vulnerable to the *ICI* due to the frequency offset introduced by the Doppler spread of the channel.

3.6 Challenges in OFDM

3.6.1 Peak-to-Average Power

The OFDM signal may exhibit a high instantaneous signal peak with respect to the average signal level. Furthermore, large signal amplitude swings are encountered, when the time domain signal traverses from a low instantaneous power waveform to a high power waveform, which may result in a high out-of-band (OOB) harmonic distortion power, unless the transmitter's power amplifier exhibits an extremely high linearity across the entire signal level range. This potentially contaminates the adjacent channels as channel interference. Therefore, a major problem associated with OFDM modulation is its large peak-to-average power ratio (*PAPR*), which makes system performance very sensitive to distortions introduced by nonlinear devices such as power amplifiers (PA). In order to mitigate the nonlinear distortion, linear PA's with a wide dynamic range are required but such PA's are inefficient.

The *PAPR* of OFDM increases exponentially with the number of subcarriers. If the power amplifiers are not operated with large power backoffs, it is impossible to keep the out-of-band power below the specified limits. This situation leads to very inefficient amplification and expensive transmitters. So it is highly desirable to reduce *PAPR*.

The *PAPR* of the transmit signal $s(n)$, is the ratio of the maximum instantaneous power and the average power, given by [37]

$$PAPR = \frac{\max_n |s_n|^2}{E_s\{|S|^2\}} \tag{3.16}$$

where $E\{\}$ denotes the expectation operator and $S = (s_0, \ldots, s_{N-1})$. Usually, the continuous time *PAPR* is estimated by the discrete time PAPR by employing the IFFT of length LN for the zero padded sequence of length LN derived from the sequence $\{ x_0, \ldots, x_{N-1}\}$, where L is the oversampling factor.

PAPR Reduction Techniques [34-37]

Several schemes have been proposed to reduce the *PAPR*. These techniques can mainly be divided into two categories: Signal distortion techniques and Signal scrambling. The signal distortion techniques reduce high peaks directly by distorting the signal prior to amplification. Clipping the OFDM signal before amplification is a simple method to limit *PAPR*. However, clipping may cause large out-of-band (OOB) and in-band interference, which results in the system *BER* performance degradation.

Signal scrambling techniques are all variations on how to scramble the codes (or modify the phases) to decrease the *PAPR*. Coding techniques can be used for signal scrambling. However, with the increase in the number of carriers, the overhead associated with exhaustive search of the best code would increase exponentially. More practical solutions of the signal scrambling techniques are block coding, selective mapping and partial transmit sequences.

Reduction of the *PAPR* by block coding the data is such that the set of permissible code words does not contain those which result in excessive peak envelope powers. However the reduction in the *PAPR* is at the expense of an increase in the bandwidth for the same data rate

and a reduction in energy per transmitted bit for the same transmit power. On the other hand, selective mapping (SLM) scheme selects a signal with minimum *PAPR* from a set of different signals as the transmit signal. While Partial transmit sequence (PTS) scheme uses the phase rotated sub-blocks into which the signal is partitioned. But both schemes are computationally complex to implement.

3.6.2. Synchronization

One of the problems facing OFDM systems is that they are highly sensitive to synchronization errors. These problems are timing and carrier frequency synchronization errors [31] [39].

Timing errors

The main idea of timing synchronization at the receiver is identifying when the symbol starts. Timing errors result in misalignment of the receiver's time-domain FFT window. The impact of the timing offset can be expressed mathematically by shifting the integration interval of Equation (3.6). For a timing error of δt, the ideal interval $t \in [kT,\ kT+T_{sym}]$ becomes $t \in [kT+\delta t,\ kT+T_{sym}+\delta t]$ and (3.6) is written as

$$y_{k,l} = \frac{1}{\sqrt{T_{sym}}} \int_{lT+\delta t}^{lT+T_{sym}+\delta t} r(t) e^{-j\frac{2\pi k(t-kT-\delta t)}{T_{sym}}} dt \qquad (3.17)$$

If δt is sufficiently small ($\delta t < T_{cp}$) to keep the channel impulse response within the cyclic prefix, the orthogonality is maintained and the receiver time FFT window will not overlap with the preceding or consecutive OFDM symbol, thus no *ISI* will arise. That is no energy is collected from adjacent OFDM symbols, and the demodulated signal constellations in Equation (3.8) in case of timing error are expressed as,

$$y_{k,l} = x_{k,l} h_{k,l} e^{-j\frac{2\pi k\delta t}{T_{sym}}} + \eta_{k,l} = x_{k,l} h_{k,l} e^{-j\frac{2\pi k\delta t'}{N}} + \eta_{k,l} \qquad (3.18)$$

where $\delta t'$ is timing error in samples. This clearly shows that timing error introduces phase rotation of the signal constellations [39]. The phase rotation is zero at the center frequency, linearly increases and is largest on the edge of the frequency band.

If coherent detection is used, the phase rotation can be taken as being introduced by the channel action, thus it will totally be detected by the channel estimation algorithm. And the subsequent equalizer will thus compensate for small amount of timing errors. However if the timing error is too large, there will be interfering energy from adjacent subcarriers leading to partial loss of orthogonality and then introducing *ISI* and *ICI*.

Frequency errors

Doppler shifts, phase noise introduced by the channel and also the difference in the transmitter and receiver oscillators create carrier frequency errors. The impact of frequency offset can be seen as an error in the frequency instants, where the received signal is sampled during demodulation by FFT. The effect of frequency offset resulting in (○) reduction in signal amplitude and (●) intercarrier interference as depicted in Figure 3.6.

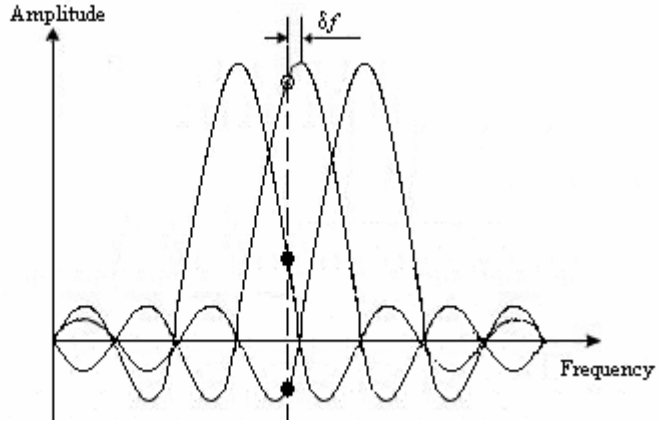

Figure 3.6 Effect of Frequency error δf

The carrier frequency error in the received signal, with simple manipulation of Equation (3.6), is expressed as,

$$y_{k,l} = e^{j(\theta+2\pi\delta flT)} \sum_{0}^{N-1} x_{k',l} h_{k',l} \frac{1}{\sqrt{T_{sym}}} \int_{0}^{T_{sym}} e^{j2\pi(\frac{k-k'}{T_{sym}}-\delta f)t} dt + \eta_{k,l} \qquad (3.19)$$

where δf is the frequency shift and θ is the phase offset created by the carrier frequency error. Due to frequency error the integral in Equation (3.19) will not equal zero for $k \neq k'$; neither does it equal one for $k = k'$. Thus orthogonality between the subcarriers has been partially lost. Further manipulation of (3.19) results into two terms; the first term indicating the equal phase rotation and attenuation of all subcarriers and the second term describes the *ICI*

$$y_{k,l} = e^{j(\theta+2\pi\delta flT)} x_{k,l} h_{k,l} \frac{1}{\sqrt{T_{sym}}} \int_0^{T_{sym}} e^{j2\pi\delta ft} dt +$$

$$e^{j(\theta+2\pi\delta flT)} \sum_0^{N-1} x_{k',l} h_{k',l} \frac{1}{\sqrt{T_{sym}}} \int_0^{T_{sym}} e^{j2\pi(\frac{k-k'}{T_{sym}}-\delta f)t} dt + \eta_{k,l} \quad (3.20)$$

The *ICI* term can be seen as an addition noise term and can thus be represented as a degradation of *SNR*.

If the frequency error is an integral n multiple of the carrier spacing Δf, then the received subcarriers are shifted by n subcarriers positions. The subcarriers are still mutually orthogonal but the received data symbols which were mapped to the OFDM spectrum are in the wrong position in the demodulated spectrum. If the frequency error is not an integer multiple of the carrier spacing, loss of orthogonality occurs creating *ICI*.

Synchronization Techniques

The synchronization system employed must perform its task within the shortest possible time at reasonable complexity and also must be able to make use of minimum number of synchronizing signals that are to be transmitted with the data signal. Usually the synchronization process is accomplished in two phases; an acquisition phase and a tracking phase. During the acquisition phase, more robust algorithms and a significant number of synchronizing signals are used to acquire an initial estimate of the errors and bring the synchronization within ±0.5 of sample time. The tracking algorithms on the other hand, have to only detect and make corrections for short duration synchronization errors [39].

There are two main methods of synchronization: pilot based and cyclic prefix based. In the first synchronization technique, the transmitter encodes reserved channels with known phases and amplitudes. Then synchronization is done by correlating the received signal in time domain or frequency domain to a copy of the synchronization signal.

There are also synchronization algorithms based on cyclic prefix [40]. Here the uncertainty in arrival time is modeled as a delay by considering a channel impulse response $h(k)=\delta(k-\theta)$,

where θ is an integer valued unknown arrival of time. And the frequency carrier offset is modeled as a complex multiplicative distortion with a factor $e^{j2\pi \varepsilon k/N}$ of the received signal, where ε denotes the carrier frequency offset. Hence the received data is $r(k) = (s(k-\theta) + \eta(k-\theta))e^{j2\pi \varepsilon k/N}$. Then, given the received signal $r(k)$ the maximum likelihood estimate of timing and frequency error is done by maximizing the likelihood function derived in [35] simultaneously for θ and ε,

$$\Lambda(\theta,\varepsilon)= \sum_{k=\theta}^{\theta+N_{cp}-1}\left(2\,\mathrm{Re}(e^{j2\pi\varepsilon}r(k)r^{*}(k+N))-\frac{SNR}{SNR+1}(|r(k)|^{2}+|r(k+N)|^{2})\right) \tag{3.24}$$

The simultaneous ML-estimation of θ and ε becoming

$$\hat{\theta} = \arg\max_{\theta}\lambda(\theta), \quad \hat{\varepsilon} = -\frac{1}{2\pi}\gamma(\theta)\Big|_{\theta=\hat{\theta}} \tag{3.21}$$

where

$$\lambda(\theta) = 2\left|\sum_{k=\theta}^{\theta+N_{cp}-1} r(k)r^{*}(k+N)\right| - \frac{SNR}{SNR+1}\sum_{k=\theta}^{\theta+N_{cp}-1}(|r(k)|^{2}+|r(k+N)|^{2})$$

and

$$\gamma(\theta) = \sphericalangle\left(\sum_{k=\theta}^{\theta+N_{cp}-1} r(k)r^{*}(k+N)\right)$$

3.6.3. Channel Estimation

In OFDM systems, the data bits are modulated on the subcarriers by some form of phase shift keying (PSK) or quadrature amplitude modulation (QAM). To estimate the bits at the receiver, knowledge is required about the reference phase and amplitude of the constellation on each subcarrier. In general, the constellation of each subcarrier shows a random phase shift and amplitude change, caused by carrier frequency offset, timing offset, and frequency selective fading. To cope with these unknown phase and amplitude variations, two different approaches exist; differential detection and coherent detection schemes.

Differential detection schemes used such as in European DAB standard [5], do not require channel estimate since the information is encoded in the difference between two consecutive symbols. This method reduces the complexity of the receiver, but there is a 3dB noise enhancement and inability to use efficient multiamplitude constellations [22]. Coherent detection, however, allows arbitrary signal constellations and is an obvious choice in wired systems where the channel hardly changes with time. In wireless systems its efficiency makes it an interesting choice when the bit rate is high, as in DVB [6].

The design of the channel estimators for wireless OFDM systems must be with both low complexity and good channel tracking ability. The choice of how the pilot tones should be transmitted is also another design criteria since the performance of the estimator depends on how pilot information is transmitted.

Channel Estimation Techniques

Various approaches are known from the literature for performing the channel estimation [41-47]; pilot-assisted, decision-directed, and blind methods. The pilot-assisted channel estimation can be performed by either inserting pilot tones into all of the sub-carriers of OFDM symbols with a specific period or inserting pilot tones into each OFDM symbol. Pilot symbol aided channel estimation might use one-dimensional (1-D), or two-dimensional (2-D) filtering algorithms.

In decision directed channel estimation method, the symbol decisions are remodulated and then employed as “pilot symbols”. The decision-directed channel parameter estimators have been used in OFDM systems for coherent detection, co-channel interference suppression, and transmitter diversity.

Blind channel estimation methods are based on the second and higher order statistics. The blind channel estimation method determines the channel transfer function without the need for the pilot symbols, however the performance has not been comparable to that of pilot based channel estimation.

3.6.4. Channel Coding

In a multipath fading channel, the received symbol is as expressed by (3.11). Accordingly, some sub-carriers will be amplified resulting in high SNR based decisions at the receiver whereas other sub-carriers will be attenuated resulting in low SNR based decisions at the receiver. In the presence of Rayleigh fading, the error rate decreases only inversely with the SNR whereas, in the absence of Rayleigh fading, the error rate decreases exponentially with the SNR [22].

In OFDM channel coding is used so that the correctly received data of the relatively strong sub-carriers corrects the erroneously received data of the relatively weak subcarriers. A number of channel coding schemes have been proposed for OFDM applications including block codes, convolutional codes, concatenated codes and turbo codes [25].

Occasional deep fades in the frequency response of the channel cause some groups of sub-carriers to be less reliable than other groups and hence cause bit errors to occur in bursts rather than independently. Since channel coding schemes are normally designed to deal with independent errors and not with error bursts then interleaving techniques are used to guarantee independence by effecting randomly scattered errors. At the transmitter, after encoding, the bits are permuted in such a way that adjacent bits are separated by several bits. At the receiver, before decoding, the reverse permutation is performed. Block or convolution interleaver can be used to accomplish this task [22]. For example, block interleavers write the bits in a matrix column by column and read the bits out from the matrix row by row.

Coding and interleaving techniques are therefore exploited to provide a link between independently fading time slots and sub-channels so that the information conveyed by well received sub-carriers corrects the information conveyed by fading sub-carriers. Note that the amount of separation in time and frequency that the interleaver ought to introduce is dictated by the coherence time and the coherence bandwidth of the channel. Particularly, to guarantee independently fading time slots and sub-channels the amount of separation in time has to be higher than the coherence time of the channel and the amount of separation in frequency has to be higher than the coherence bandwidth of the channel.

3.7 MCM versus Single-Carrier Transmission

The *BER* of an OFDM system is dependent on several factors, such as the modulation scheme used, the amount of multipath, and the level of noise in the signal. However if we look at the performance of OFDM with just AWGN then the performance of OFDM is exactly the same as that of a single-carrier coherent transmission using the same modulation scheme. Moreover, the efficiency of FFT algorithms implemented in OFDM also makes the computational complexity much less than the time-domain equalization in a single-carrier system.

However, most propagation environments suffer from the effects of multipath propagation. For a given fixed transmission bandwidth, the symbol rate for a single carrier transmission is very high, where as for an OFDM signal it is N times lower, where N is the number of subcarriers used. This lower symbol rate results in a lowering of the *ISI*. In addition to lowering of the symbol rate, OFDM systems also uses a cyclic prefix at the start of each symbol. This cyclic prefix removes any *ISI* shorter than its length. If the guard period is sufficiently long, then all the *ISI* can be removed.

Multipath propagation results in frequency selective fading that leads to fading of individual subcarriers. Most OFDM systems use Forward Error Correction to compensate for the subcarriers that suffer from severe fading. The additional spectral efficiency of those subcarriers that have a *SNR* greater than the average (due to constructive interference) tends to compensate for subcarriers that are subjected to fading (destructive interference). As a result of this the performance of such an OFDM system in a multipath environment can be made to approach its performance in an AWGN channel [48]. However, the performance of a single carrier transmission will degrade rapidly in the presence of multipath propagation.

For a multi-carrier system, such as OFDM, the envelope fluctuation is large. A signal with large envelope fluctuation requires a power amplifier with large backoff, which makes the amplifier power inefficient. Therefore, the power amplifier for a single-carrier system has a good power efficiency compared with that for an OFDM system.

Chapter 4

Discrete Wavelet Transform

4.1. Overview

Representations of a signal in a suitable way for a specific application are obtained by decomposing the signal with a suitable algorithm. Here, the decomposition must have a fast algorithm for implementation and the resulting signal representations must have a specific physical interpretation [49].

The Fourier transform is one of the classical tools used to achieve such representations of a signal. For a given signal $x(t)$, while the Fourier-based method will isolate peaks at certain frequency, it provides no time localization. This means the original signal $x(t)$ is completely specified in time with no frequency content while in its Fourier transform $X(\omega)$, the frequency content of the signal is known, but no information is given regarding where these frequencies occur in time. To provide a certain level of time localization, a variant of Fourier transform, obtained by time windowing is used, termed as short-time Fourier transform (STFT). Still in STFT both time and frequency localizations are fixed.

The idea behind time-frequency representation is to decompose the signal of interest into several subbands and analyze each subband separately. But obtaining arbitrarily fine time-frequency resolution, in the representation of a signal, is not possible due to the uncertainty principle. That is, it is not possible to represent a signal with a point in time-frequency space. Wavelet transform, with all the translated and dilated versions of the analyzing function, provides a near arbitrary time-frequency resolution or localization [53-55]. The frequency

resolution provided by wavelet transform is logarithmic, that is time resolution gets finer in the highest frequency.

Wavelet analysis, based on multiresolution analysis, subband coding and filter bank implementation have been shown to have different applications. We can mention an array of such different applications but as we are here interested in its application for multicarrier modulation (*MCM*) in digital communication [55-57], we will explore this in the following sections.

4.2. Continuous Wavelet Transform [51],[52],[56],[58]

The wavelet transform typically uses translations (shifts) and dilations (scales) of one fixed function, the mother wavelet $\psi \in L_2(\mathbf{R})$. In case of continuous wavelet transform, the translation and dilation parameters vary continuously. The wavelet is defined as,

$$\psi_{s,\tau}(t) = \frac{1}{\sqrt{s}} \psi\left(\frac{t-\tau}{s}\right) \tag{4.1}$$

where s is the scale factor, inverse of frequency, corresponding to the frequency information of the signal and τ is the translation factor related to the location of the wavelet as it is shifted through the signal providing time information. These functions are normalized to have a constant L_2 norm. One of the simplest wavelets with an explicit formula is the Haar wavelet, depicted in figure 4.1, along with its Fourier transform as

$$\psi_{Haar}(t) = \begin{cases} 1 & 0 \le t \le 1/2 \\ -1 & 1/2 \le t \le 1 \\ 0 & otherwise \end{cases} \tag{4.2a}$$

$$\Psi_{Haar}(\omega) = j e^{-j\omega/2} \frac{\sin^2(\omega/4)}{\omega/4} \tag{4.2b}$$

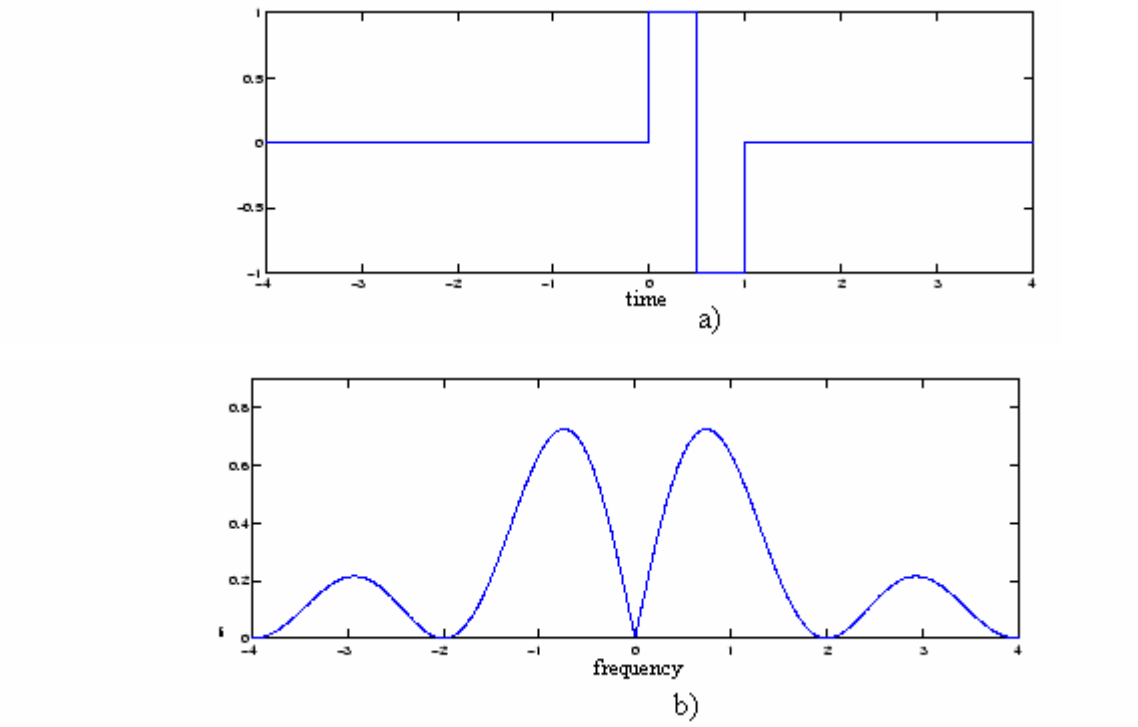

Figure 4.1 The Haar Wavelet (a) and its Fourier transform (b)

Starting with a particular analyzing(mother) wavelet ψ and a signal of interest $x(t)$, the continuous wavelet transform (*CWT*) can be interpreted as the decomposition representation of the signal with respect to the wavelet family generated by the translated and dilated versions of the analyzing wavelet function ψ . More formally it may be expressed as

$$\mathcal{W}(s,\tau) = \langle x, \psi_{s,\tau} \rangle = \int x(t)\psi_{s,\tau}(t)dt \qquad (4.3)$$

The *CWT* $\mathcal{W}(s,\tau)$ may also be interpreted as the output of a bank of linear filters which are constructed by the dilation/contraction of $\psi(t)$. The filter corresponding to dilated version of $\psi(t)$ respond to lower-frequency content of the signal, while the one related to contracted version of $\psi(t)$ respond to higher-frequency content.

Using Parseval's identity, the transform can also be written as

$$2\pi\mathcal{W}(s,\tau) = \langle X, \Psi_{s,\tau} \rangle \qquad (4.4)$$

where X and $\Psi_{s,\tau}$ are Fourier transforms. Now with the assumption that the wavelet $\psi(t)$ and its Fourier transform $\Psi_{s,\tau}$ are functions with finite centers $\bar{t}$ and $\overline{\omega}$ and finite radii Δ_t and Δ_ω, given as

$$\bar{t} = \frac{1}{\|\psi\|^2} \int_{-\infty}^{\infty} t|\psi(t)|^2 dt \tag{4.5a}$$

$$\Delta_t = \frac{1}{\|\psi\|^2} \int_{-\infty}^{\infty} (t-\bar{t})^2 |\psi(t)|^2 dt \tag{4.5b}$$

and similarly for $\overline{\omega}$ and Δ_ω.It is clear that from (4.2) and (4.3), the *CWT* at (s,τ) picks up information about the signal, in particular from the time interval [$\tau + s\bar{t} - s\Delta_t$, $\tau + s\bar{t} + s\Delta_t$] and from the frequency interval [($\overline{\omega} - \Delta_\omega$)/$s$, ($\overline{\omega} + \Delta_\omega$)/$s$]. These two intervals determine the time-frequency tile; whose width, height and position are determined by s and τ.

The generating wavelet function ψ is selected in such a way that it satisfies the admissibility condition,

$$C_\psi = \int_{-\infty}^{\infty} \frac{|\Psi(\omega)|}{\omega} d\omega \; < \infty \tag{4.6a}$$

in order to analyze and then reconstruct the signal without loss of information. The admissibility condition implies that the Fourier transform of $\psi(t)$ vanishes at zero frequency, i.e.

$$|\Psi(\omega)|^2 \Big|_{\omega=0} = 0 \tag{4.6b}$$

This means the wavelet $\psi(t)$ must have a bandpass spectrum. The mean in time domain must also be zero,

$$\int \psi(t) dt \; = 0 \tag{4.6c}$$

Then, the continuous wavelet transform $\mathcal{W}(s,\tau)$ is invertible on its range, and the inverse transform is given by the relation

$$x(t) = \frac{1}{C_\psi} \int_{-\infty}^{\infty} \int_{-\infty}^{\infty} w(s,\tau)\psi_{s,\tau}(t) \frac{ds d\tau}{s^2} \tag{4.7}$$

The continuous wavelet transform allows us to use a very general wavelet. At the other extreme, we shall see that much more restrictive conditions hold for a wavelet used in multiresolution analysis. This allows us, on the other hand, to obtain powerful results such as the construction of orthogonal bases.

4.3. Discrete Wavelet Transform [51],[52],[56],[58]

4.3.1. Discretization of the CWT

The CWT as defined in (4.2) is a two-dimensional function defined over the time-frequency plane by continuously shifting a continuously scalable function over the signal and calculating the correlation between the signal and the scaled functions. This results in an infinite number of scaled wavelet functions, which are not orthogonal and thus highly redundant [52].

Furthermore, for most functions the continuous wavelet transform have no analytical solution which means they can only be calculated numerically. This problem of CWT can be overcome by restricting the scale and translation factors to be discrete. Now the wavelet function of (4.1) is appropriately defined as

$$\psi_{m,n}(t) = s_0^{-m/2} \psi_{m,n}\left(s_0^{-m} t - n\tau_0\right) \tag{4.8a}$$

where $m,n \in \mathbf{Z}$, $s_0 > 1$ is a fixed dilation step and τ_0 is a translation factor dependent on the dilation step. The use of fixed dilation steps corresponds to the sampling of the time-frequency plane at discrete intervals. The commonly used method of discretizing the CWT is by using dyadic grid. Thus with dyadic sampling, that is $s_0 = 2$ and $\tau_0 = 1$, (4.8a) represents a discrete wavelet function expressed as

$$\psi_{m,n}(t) = 2^{-m/2} \psi_{m,n}\left(2^{-m} t - n\right) \tag{4.8b}$$

4.3.2 Multiresolution Analysis

Using the discrete wavelets given by (4.8b), the wavelet series decomposition and reconstruction are given by

$$w_{m,n} = \int_{-\infty}^{\infty} x(t)\psi_{m,n}(t)dt \tag{4.9a}$$

$$x(t) = \sum_m \sum_n w_{m,n}\psi_{m,n}(t) \tag{4.9b}$$

This naturally leads to multiresolution analysis described as follows:

Define W_m to be the set of all signals $x(t)$, which can be synthesized from the wavelets $\psi_{m,n}(t)$. These spaces are orthogonal to each other and we can synthesize any signal, $x(t)$ as

$$x(t) = \sum_{m=-\infty}^{\infty} x_m(t) \text{ where } x_m(t) = \sum_{n=-\infty}^{\infty} w_{m,n}\psi_{m,n}(t) \tag{4.10a}$$

Next define V_m to be the set of all signals $x(t)$, which can be synthesized from the wavelets $\psi_{i,n}(t)$ where $i < m$ and $-\infty < n < \infty$ as

$$x(t) = \sum_{i=-\infty}^{m-1} \sum_n w_{i,n}\psi_{i,n}(t) \tag{4.10b}$$

The spaces V_m are nested inside each other,

$$V_m \subset V_{m+1}$$

with $\bigcap_{m\in Z} V_m = \{0\}$ and $\overline{\bigcup_{m\in Z} V_m} = L_2(\mathbf{R})$, where the over bar indicates closure. That is, as j goes to infinity V_m enlarges to become all energy signals $L_2(\mathbf{R})$. And as m goes to negative infinity V_m shrinks down to the zero signal. Thus, each subspace V_m is the m-th level approximation to the space $L_2(\mathbf{R})$.

In multiresolution analysis (MRA), the subspace V_0 is used as a reference space, usually, to which all other resolutions are related (by dilation of power of two). Hence,

$$x(t) \in V_m \implies x(2t) \in V_{m+1}$$

It is clear from the definitions of the spaces that every signal in V_{m+1} is a sum of a signal in V_m and W_m since

$$x(t) = \sum_{i=-\infty}^{m} \sum_{n} w_{i,n}\psi_{i,n}(t) = \sum_{i=-\infty}^{m-1} \sum_{n} w_{i,n}\psi_{i,n}(t) + \sum_{n} w_{m,n}\psi_{m,n}(t) \qquad (4.11)$$

That is, we can write

$$V_{m+1} = W_m \oplus V_m$$

This shows that the spaces W_m are the differences between adjacent spaces V_m and V_{m+1}. This idea results in various decompositions of the signal $x(t)$, as defined by the breakdown

$$\begin{aligned} V_0 &= V_{-1} + W_{-1} \\ &= V_{-2} + W_{-2} + W_{-1} \\ &\vdots \end{aligned} \qquad (4.12)$$

which can now be written for two levels as

$$\begin{aligned} x(t) &= A_1(\mathrm{t}) + D_1(\mathrm{t}) \\ &= A_2(\mathrm{t}) + D_2(\mathrm{t}) + D_1(\mathrm{t}) \\ &\vdots \end{aligned} \qquad (4.13)$$

where Where D_i(t), in W_{-i} , is called the detail at level i and A_i(t), in V_{-i}, is called the approximation at level i.

4.3.3 The Scaling Function

The multiresolution analysis leads to a scaling function, a pair of discrete time filters, and a perfect reconstruction filter bank which can be used to calculate the DWT. A function $\phi \in V_0$ exists, called scaling function, such that the collection $\{\phi(t-n) \mid n \in \mathbf{Z}\}$ is orthonormal basis of V_0.

Since $\phi \in V_0 \subset V_1$, a sequence $\{h_0(n)\} \in \ell_2$ (ℓ_2 is the space of finite energy sequences) exists so that the scaling function satisfies the dilation equation [58]

$$\phi(t) = 2^{1/2} \sum_{n} h_0(n)\phi(2t-n) \qquad (4.14)$$

where $h_0(n)$ are coefficients of the scaling function. It also follows immediately that the collection of functions $\{\phi_{m,n}(t)=2^{m/2}\phi(2^m t-n)|\ m,\ n\in\mathbf{Z}\}$, with, is an orthonormal basis of V_m.

To be able to use the collection $\{\phi(t-n)|\ n\in\mathbf{Z}\}$ to approximate even the simplest of functions, it is natural to assume that the scaling function and its integer translates form a partition of unity,

$$\forall t \in \mathbf{R}: \quad \sum_k \phi(t-n)=1 \tag{4.15}$$

Then MRA asserts that there exists a function ψ, called the mother wavelet, explicitly computable from the scale function ϕ, such that $\{\psi_{m,n}(t)=2^{m/2}\psi(2^m t-n),\ m,\ n\in\mathbf{Z}\}$ forms an orthonormal basis of $L_2(\mathbf{R})$. These are what are normally termed as *orthonormal wavelets*.

Taking the Fourier transform of (4.14),

$$\Phi(\omega) = \frac{1}{\sqrt{2}} H_0\left(e^{j\omega/2}\right)\Phi\left(\frac{\omega}{2}\right) \tag{4.16}$$

where

$$H_0\left(e^{j\omega}\right) = \sum_{n=-\infty}^{\infty} h_0(n)e^{jn\varpi}$$

is 2π periodic discrete-time Fourier transform of the scaling coefficients $h_0(n)$. Now by observing that the wavelet basis function $\psi \subset W_0 \subset V_0$, with the relation

$$\Psi(\omega) = \frac{1}{\sqrt{2}} e^{-j\omega/2} H_0^*\left(e^{j(\omega/2+\pi)}\right)\Phi\left(\frac{\omega}{2}\right) \tag{4.17}$$

whose inverse gives the wavelet basis function

$$\psi(t) = 2^{1/2}\sum_n h_1(n)\phi(2t-n) \tag{4.18}$$

where $h_1(n)$ are coefficients of the wavelet basis, related to the scaling function coefficients $h_0(n)$ as

$$h_1(n) = (-1)^n h_0(-n+1) \tag{4.19}$$

The orthogonality conditions for the scaling and wavelet basis functions are stated as

- The scaling functions are orthonormal across their translates,

$$\left\langle \phi_{m,n}(t), \phi_{m,n'}(t) \right\rangle = \delta[n-n'] \tag{4.20a}$$

- The wavelet basis functions are orthonormal across their translates and dilations,

$$\left\langle \psi_{m,n}(t), \psi_{m',n'}(t) \right\rangle = \delta[m-m']\delta[n-n'] \tag{4.20b}$$

- the wavelet basis is orthogonal to the scaling function

$$\left\langle \psi_{m,n}(t), \phi_{m',n'}(t) \right\rangle = 0 \quad \forall\ m,n,m',n' \tag{4.20c}$$

The orthogonality conditions in (4.20) together with (4.19) give

$$\sum_n h_0(n) h_0(n+2k) = \delta(k) \tag{4.20d}$$

which is the same as that for perfect reconstruction(PR) conditions of quadrature mirror filter, where the zero-mean highpass filter sequence $\{h_1(n)\}$ is the mirror image of lowpass $\{h_0(n)\}$.

Here also, the simplest wavelet, Haar wavelet, scaling function is expressed as

$$\varphi(t) = \phi(2t) + \phi(2t-1) = \frac{1}{\sqrt{2}}\sqrt{2}\phi(2t) + \frac{1}{\sqrt{2}}\sqrt{2}\phi(2t-1) \tag{4.21a}$$

the scale function coefficients being $h_0(n) = \left[\frac{1}{\sqrt{2}}, \frac{1}{\sqrt{2}}\right]$, and the wavelet function (4.2a), is given as

$$\psi(t) = \phi(2t) - \phi(2t-1) = \frac{1}{\sqrt{2}}\sqrt{2}\phi(2t) - \frac{1}{\sqrt{2}}\sqrt{2}\phi(2t-1) \tag{4.21b}$$

the corresponding coefficients being $h_1(n) = \left[\frac{1}{\sqrt{2}}, -\frac{1}{\sqrt{2}}\right]$

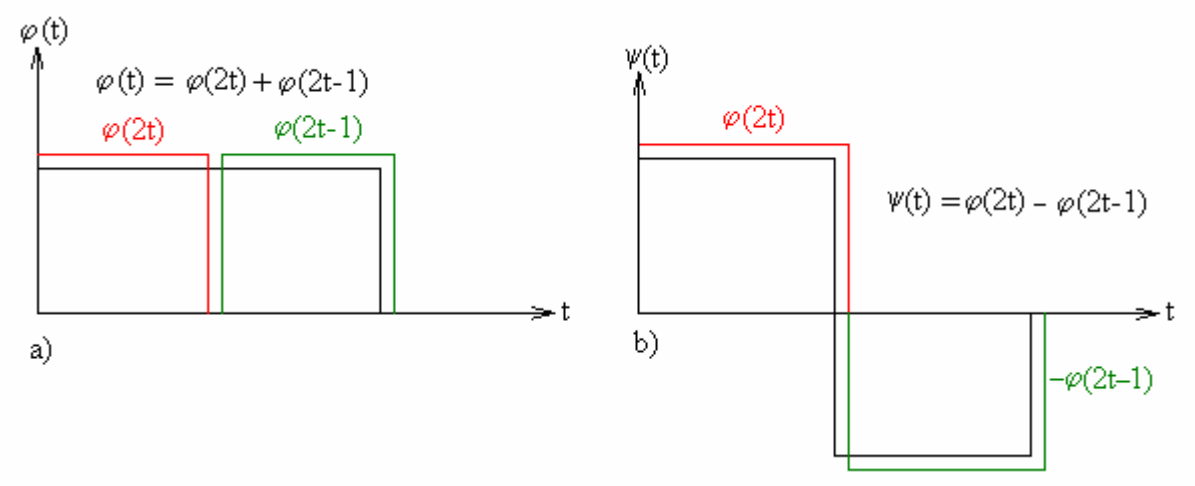

Figure 4.2 The Haar Scaling (a) and wavelet (b) function

4.3.4 Filter bank Implementation [52-53], [59]

The construction of orthonormal basis functions based on the multiresolution analysis is direct continuous-time approach. The construction of the orthonormal basis functions from a prototype wavelet can also be carried out using discrete-time filters. The filters can be iterated and under certain conditions lead to continuous-time wavelets. This construction method results in a very practical wavelet decomposition schemes, since they are implemented with a finite length discrete-time filters.

The coefficients $h_0(n)$ (4.14) and $h_1(n)$ (4.18) denote lowpass and highpass filters respectively. The filter bank is iterated on the lowpass branch (see Figure 4.3) and the process is iterated to infinity. The two filters after the *i-th* iteration are expressed, in z-domain, as

$$H_0^{(i)}(z) = \prod_{k=0}^{i-1} H_0\left(z^{2^k}\right) \qquad (4.22)$$

$$H_1^{(i)}(z) = H_1\left(z^{2^{i-1}}\right)\prod_{k=0}^{i-1} H_1\left(z^{2^k}\right), \qquad i=1, 2,\ldots$$

These filters are preceded by upsampling by 2^i (Here at the first iteration $H_0^{(0)}(z)=H_1^{(0)}(z)=1$). The corresponding continuous time iterated functions $\phi^i(t)$ and $\psi^i(t)$ with the associated discrete-time iterated filters $h_0^i(n)$ and $h_1^i(n)$

$$\phi^i(t) = 2^{i/2} h_0^i(n), \quad n/2^i \le t < \frac{n+1}{2^i} \tag{4.23a}$$

$$\psi^i(t) = 2^{i/2} h_1^i(n), \quad n/2^i \le t < \frac{n+1}{2^i} \tag{4.23b}$$

The length of the iterated filter $h_0^i(n)$ with length L filter $h_0(n)$ is $L^{(i)} = (2^i - 1)(L - 1) + 1$, which becomes infinite as $i \to \infty$. The normalization of the interval by 2^i insures that $\phi^i(t)$ stays compactly supported within $[0, L - 1]$.

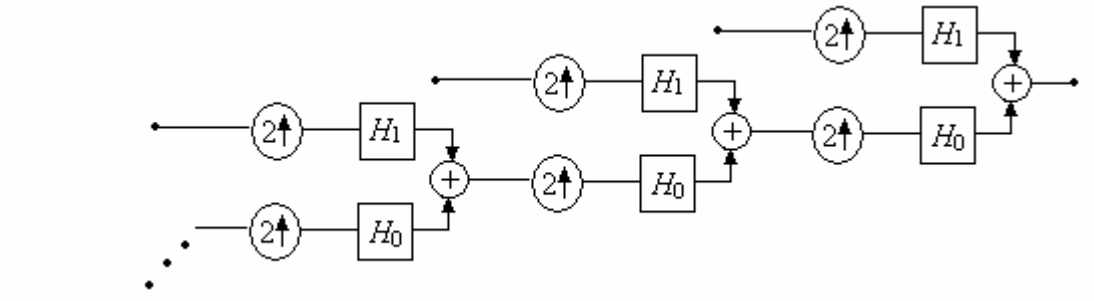

Figure 4.3 Two channel filter bank (Synthesis Part)

In Fourier domain, defining $M_0(\omega) = 2^{-1/2} H_0(e^{j\omega})$ and $M_1(\omega) = 2^{-1/2} H_1(e^{j\omega})$, the scaling function and wavelet function in (4.16) and (4.17) can be written as,

$$\Phi(\omega) = \lim_{i \to \infty} \Phi^i(\omega) = \prod_{k=1}^{\infty} M_0\left(2^{-k}\omega\right) \tag{4.24a}$$

$$\Psi(\omega) = \lim_{i \to \infty} \Psi^i(\omega) = M_1(\omega/2) \prod_{k=2}^{\infty} M_0\left(2^{-k}\omega\right) \tag{4.24b}$$

For perfect reconstruction together with orthogonality (4.20d)

$$\left|M_0(e^{j\omega})\right|^2 + \left|M_0(e^{j(\omega+\pi)})\right|^2 = 1 \tag{4.25a}$$

And for the regularity,

$$M_0(\omega) = \left[\frac{1}{2}\left(1 + e^{j\omega}\right)\right]^N R(j\omega), \quad \text{where } R(j\omega) \text{ is remainder} \tag{4.25b}$$

This implies that the wavelet have N vanishing moments that is

$$\int t\psi(t)dt\ ,\ \int t^2\psi(t)dt\ ,\ldots\ldots,\ \int t^N\psi(t)dt$$

with a support ($2N - 1$). The filters have $2N$ nonzero coefficients. As N increases the wavelet becomes increasingly smooth.

Figure 4.4 shows the Daubechies scaling and wavelet function representations for the first eight iterations of a length-8 filter with support 7 and length-16 filter with support 15. The construction of Daubechies family orthonormal wavelets is briefly given in [46].

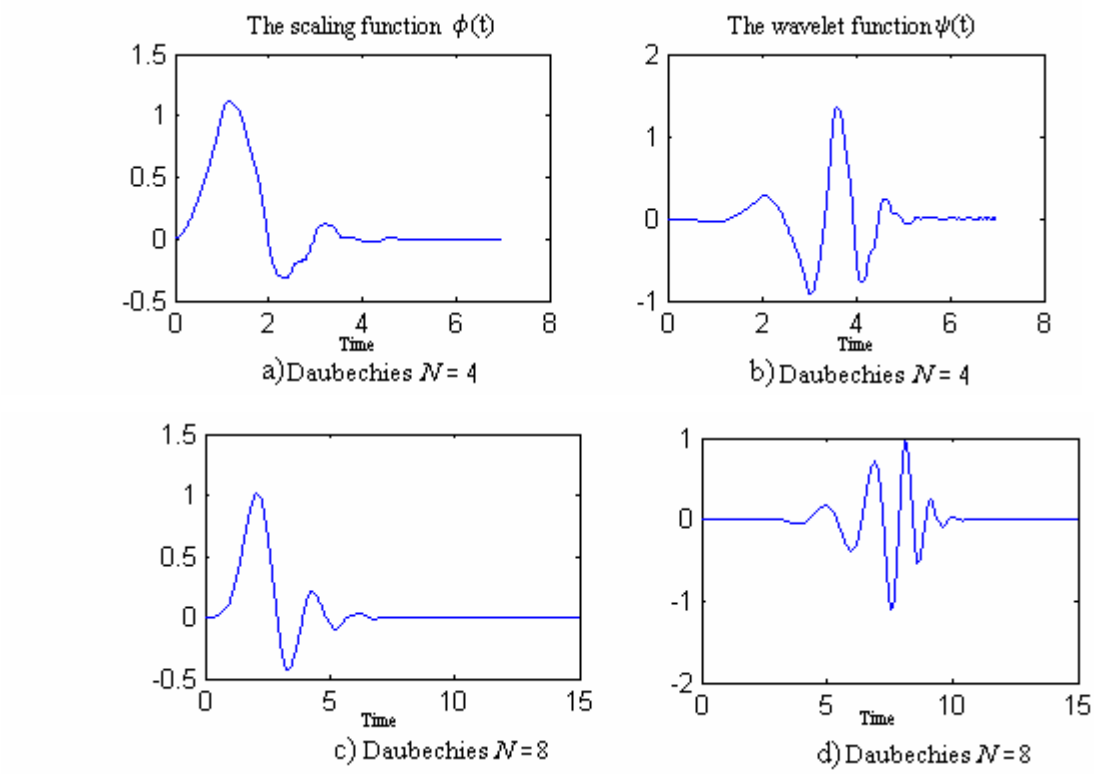

Figure 4.4 8-iterations of orthonormal 4-tap and 8-tap Daubechies scaling and wavelet functions

4.4 Wavelet Based OFDM

In wavelet-based OFDM, the IFFT and FFT blocks are simply replaced by an inverse discrete wavelet transform (IDWT) and discrete wavelet transform (DWT), respectively [13]. In Fourier- based OFDM, there are M independent QAM subchannels via a $K = 2M$ point IFFT

operation (when the conjugate symmetry condition is imposed). The real wavelet transform, converts real numbers to real numbers, and hence real constellation must be used in each subchannel. To keep the same data rate in wavelet systems, K independent subchannels are multiplexed together via a *K* point IDWT.

Perfect spectral containment requires ideal brickwall filters, which are not physically realizable due to the infinite length of their impulse responses. It is desirable, however, to be as close as possible to brickwall filters, to have a high degree of spectral containment, and limit the effects of *ICI*. The filter bank structure accomplishing this multicarrier modulation by DWT is shown in Figure 4.5.

Daubechies compactly supported wavelets are used for the implementation. Thus the filters are of finite impulse response whose coefficients are derived as explained in section 4.3.4. The analysis and synthesis filters are in time reverse relationship; this together with the identity in Equation (4.25a) makes the filters perfect reconstruction filters.

In OFDM employing Fourier filters, the overlap factor is equal to 1, thus the pulse waveforms for different symbol blocks do not overlap in time. However, for wavelet OFDM, the overlap factor is greater than 1, hence the pulse waveforms overlap in time. In Fourier filter banks, the prototype filter is simply a rectangular window. In the wavelet case the set of *N* bandpass pulses ψ_k ; $0 \le k \le N$-1 and their time-shifts by integer multiples of *N*, provide an orthonormal set of waveforms for transmission of the sequence of symbol blocks [13].

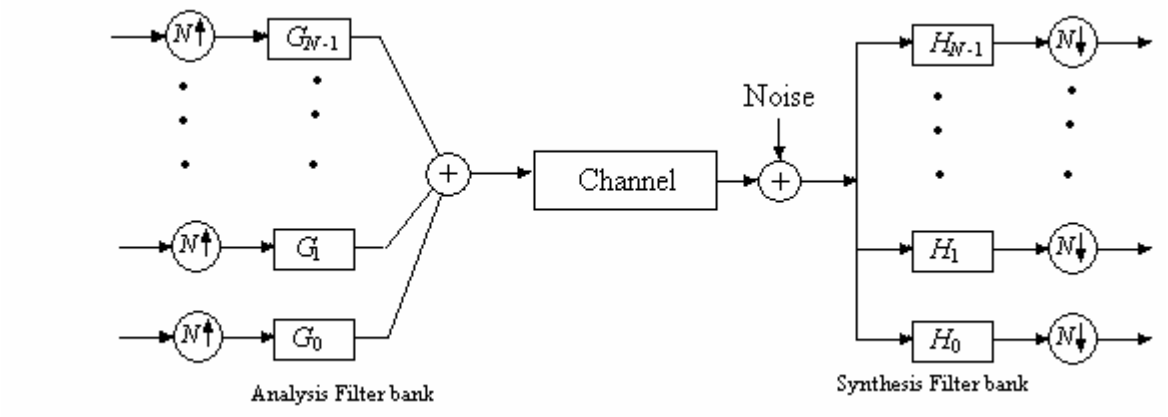

Figure 4.5 Wavelet based MCM Structure

Due to higher spectral containment between subchannels, wavelet-based OFDM is better able to overcome the effects of narrowband interference and is inherently more robust with respect to *ICI* than traditional Fourier filters [13]. Wavelet OFDM is implemented via overlapped waveforms to preserve data rate. Thus the use of cyclic prefix does not make sense in this context. Without the cyclic prefix, the data rate in wavelet systems can surpass those of Fourier implementations, one of its key motivating factors.

Computational complexity is another key issue. Due to the high data rates required in modern applications, low complexity is imperative. Both Fourier and wavelet (for which there is a uniform frequency decomposition) transforms have a computational complexity of $O(N\log N)$, where N is the rank of the transform, or the number of subchannels [52].

The main sidelobe of the Fourier filter has a magnitude 13dB smaller than the main lobe. For the wavelet filter, on the other hand, the first sidelobe has a magnitude 40dB below the main lobe [13].The great reduction in sidelobe levels is the main motivation behind the recent trend of using wavelet filters in OFDM systems. Wavelet filters provide better spectral containment than their Fourier counterparts. When orthogonality between carriers is lost, after the transmitted signal passes through a non-uniform channel, the amount of interference between carriers in wavelet systems is much lower than in Fourier systems, since the sidelobes contain much less energy. The improved spectral containment reduces *ICI*. Reduced *ICI* without the need for a cyclic prefix is an attractive feature of wavelet OFDM. It allows data rates to be pushed past those of Fourier OFDM, which relies heavily on the cyclic prefix and 1-tap equalizer to mitigate the effects of *ICI*.

Chapter 5

Simulations and Results

5.1. Simulation Setup

In this thesis study, a baseband OFDM scheme, as shown in Figure 5.1, is implemented in MATLAB environment. Both the DFT-based and wavelet-based MCM schemes are implemented and their comparative performance study is carried out under different channel scenarios. The measure of performance used is bit error rate versus signal-to-noise ratio (*BER* vs. *SNR*). The implemented program simulates a 64 subcarrier OFDM system. Constellation mapping or message modulation is performed using two schemes, quadrature amplitude modulation (QAM) for FFT and their equivalent pulse amplitude modulation (PAM) for DWT. The additive white gaussian noise (AWGN) channel model is used as the starting point for this study, also the flat Rayleigh fading and frequency selective fading channel models with AWGN are also considered. The simulation parameters are summarized in table 1.

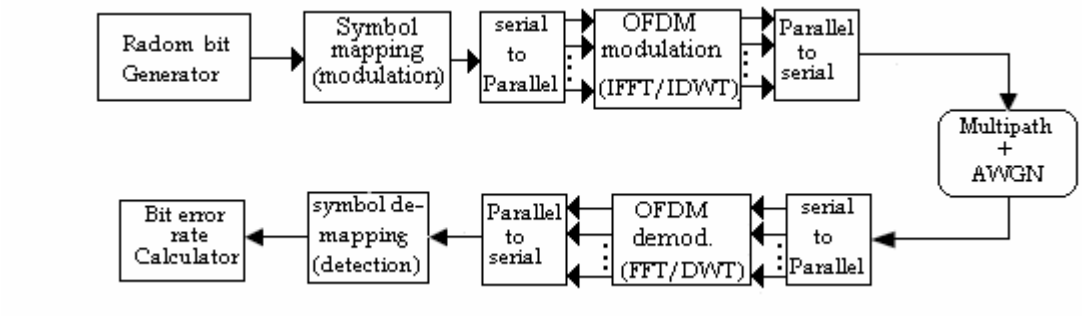

Figure 5.1 Block diagram of the system Implemented

5.1.1. Description of the simulation model

The Transmitter

- Random bit Generator

Used for generating the random information bits. It uses standard random bit generator and generates random data vector for transmission.

- Symbol Mapping

This block is used for baseband modulating the random bits using one of the schemes PSK and QAM for DFT-based scheme and PAM for DWT-based scheme.

- Serial to Parallel

This block reshapes the baseband modulated data vector into parallel column vectors before being mapped into each subcarrier.

- OFDM Modulation

The subcarrier mapping is accomplished by using inverse fast Fourier transform (IFFT) and inverse discrete wavelet transform (IDWT).

- 64 subcarriers are used with a total bandwidth of 20MHz giving a sample time of 0.05μsec.
- For both OFDM schemes the same amount of random data bits are generated and used for the system simulation and analysis.
- The bit rate value for OFDM is given by

$$\text{No of subcarriers} \times \text{Coding Rate} \times \frac{No\ of\ coded\ bits}{Subcarrier\ symbol} \times \frac{1\ subcarrier\ symbol}{symbol\ period} \quad (5.1)$$

For uncoded 64subcarrier, 16sample cyclic prefixed DFT based OFDM the symbol period is 4μsec. Thus, the bit rate for BPSK modulation becomes 16Mbps. While for that of DWT-based scheme the symbol period is 3.2μsec, thus for the same modulation the bit rate is 20Mbps. Thus, the DWT-based scheme is operated at a 25% higher bit rate for all modulation types.

- Parallel to Serial

This block changes the OFDM modulated symbols into serial stream for transmission.

* Cyclic Prefix of 16sample interval is inserted on the DFT-based scheme while the DWT-based scheme is transmitted without any guard interval insertion.

The Receiver

The received serial data is converted into parallel and demodulated using FFT/DWT and then converted back to serial for baseband demodulation PSK,QAM or PAM demodulators. Finally bit error computation is done as

- For every signal-to-noise ratio value, the error probability is estimated as

$$Pe = \frac{No\ of\ errors}{Total\ No\ of\ symbols} \tag{5.2}$$

And the BER results are taken as an average of 10 independent trials.

- All the simulations are carried out using MatLab Version 7(R14) program on Intel Pentium4 2.4GHz processor, 256MB RAM computer running Windows XP operating system.

Table 5.1 Simulation parameters

Parameters	Set Value
Number of DFT/DWT points	64
Bandwidth	20MHz
Modulation/Demodulation	BPSK 4QAM / 4PAM
Channel Environment	AWGN Flat Rayleigh Fading + AWGN Frequency selective Rayleigh Fading + AWGN

Figure 5.2 below shows the transmitted OFDM signal spectrum. The digital-to-analog and analog-to-digital converters DAC/ADC systems used in the actual passband system introduce dc offset and may attenuate the subcarrier centered at dc. And also the low pass filters used within the DAC/ADC will attenuate the subcarriers near the Nyquist sampling frequencies $f_s/2$. The spectrum clearly shows that the subcarrier at dc and some subcarriers at the edges of the spectrum are removed.

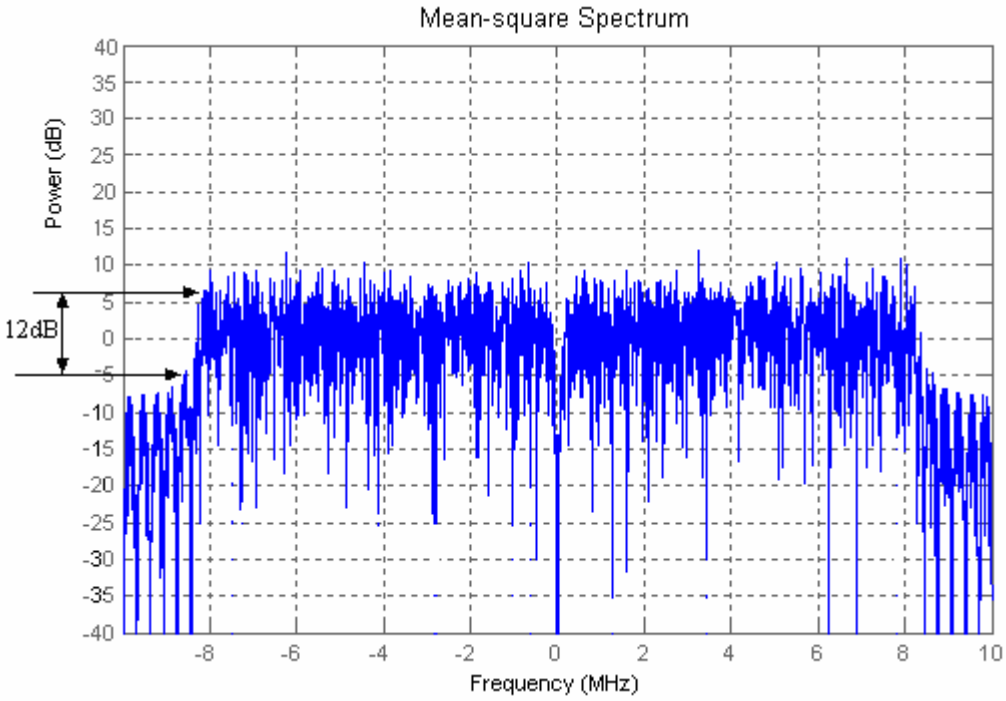

Figure 5.2 Average power spectrum of DFT-based MCM implementation

5.1.2. The channel

AWGN

A complex white gaussian noise is added to the transmitted MCM signal. The noise is generated by a gaussian random noise generator with variance dependent on the input signal-to-noise ratio parameter specified for simulation.

Multipath Fading channel

The baseband signal is faded by Rayleigh fading multipath generator, and white complex gaussian noise is added. The Rayleigh fading envelops are generated using Clark's model as discussed in section 2.4. First complex gaussian noise samples will be generated and are filtered by $H(f)=\sqrt{S_{Ez}(f)}$

$$S_{Ez}(f) = \frac{1}{\pi f_m \sqrt{1-((f-f_c)/f_m)^2}} \qquad (5.3)$$

where f_c is the carrier frequency (IEEE 802.11a's 5.2GHz is used), f_m is the maximum Doppler frequency. Then passed through IFFT filters and added in quadrature to produce the

complex Rayleigh fading envelops. And Figure 5.4(a) and 5.4(b) show the plot the Raleigh fading output generated using this model.

The frequency selective fading channel is modeled as Rayleigh fading tap delay line with exponentially decaying profile.

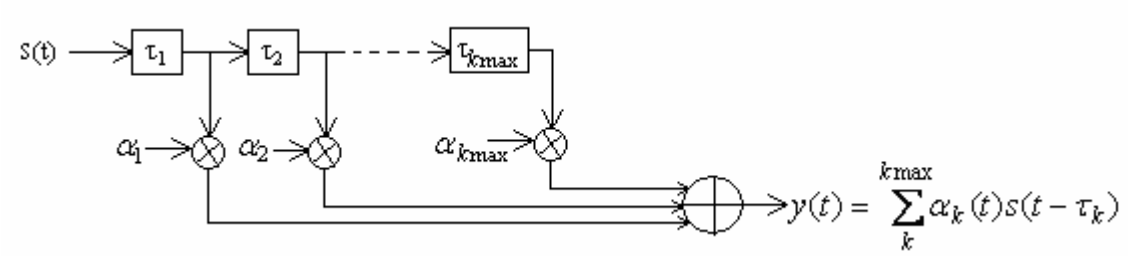

Figure 5.3 The Tapped delay line model

The probability distribution of the *k*-th tap of the channel impulse response h_k is given by $N(0,\frac{1}{2}\sigma_k^2)+jN(0,\frac{1}{2}\sigma_k^2)$, where $N(0,\frac{1}{2}\sigma_k^2)$ is a zero-mean Gaussian random variable with variance $\frac{1}{2}\sigma_k^2$, τ_{RMS} is the RMS delay spread, and T_s is the sampling time. The energy of each channel tap is given by:

$$\sigma_k^2 = \sigma_0^2 e^{-kT_s/\tau_{RMS}} \tag{5.4}$$

where σ_0^2 is chosen in such a way as to ensure that average received energy is unity:

$$\sigma_0^2 = \frac{1-e^{-T_s/\tau_{RMS}}}{1-e^{-(k_{\max}+1)T_s/\tau_{RMS}}} \tag{5.5}$$

and the link performances are analyzed at different delay spread.

The receiver performs a subcarrier demodulation on the received signal using FFT or DWT, then, demodulation of the constellation will be carried out. Finally error calculation will be done for performance comparison.

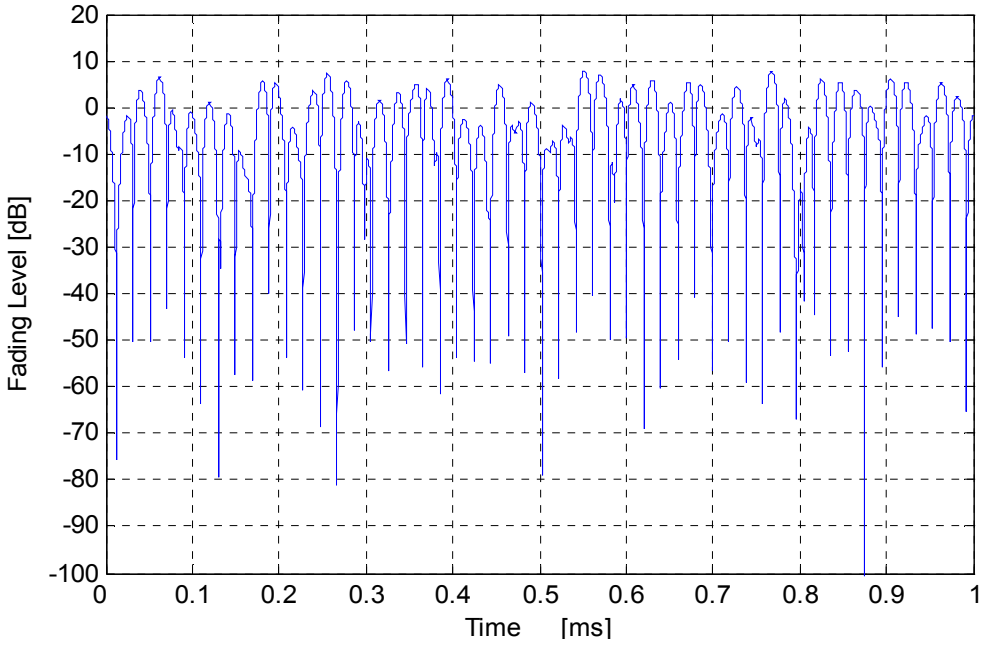

Figure 5.4(a) A typical Rayleigh fading envelop simulated at 25Hz Doppler.

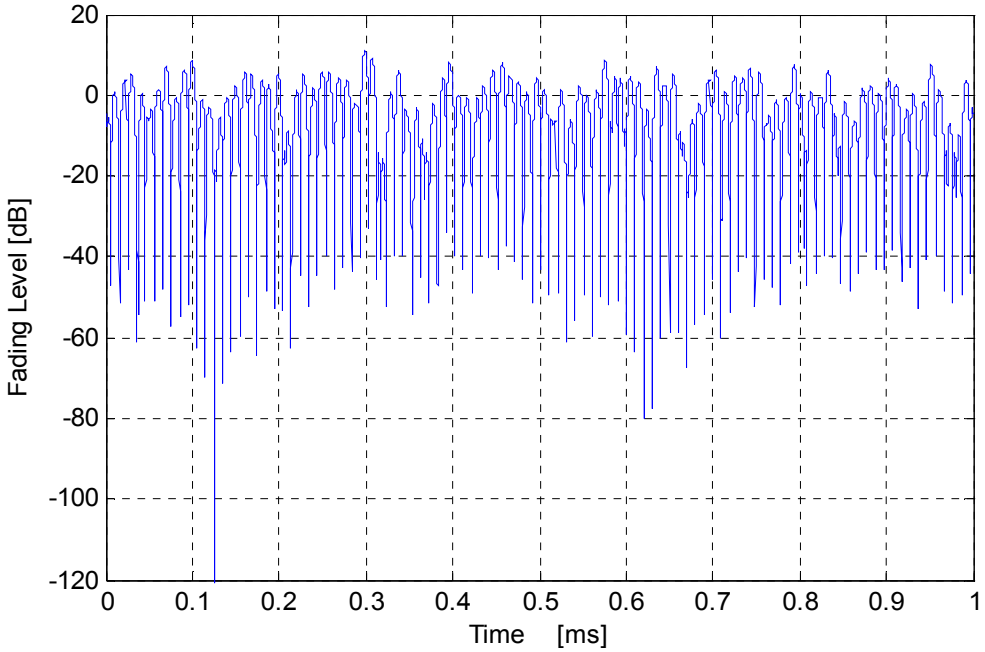

Figure 5.4(a) A typical Rayleigh fading envelop simulated at 120Hz Doppler.

- The simulation is done using the assumption of perfect synchronization both in time and in frequency, and also perfect channel knowledge.

5.2. AWGN channel Performance

The *BER* vs. *SNR* performance of both the DFT-based and DWT-based MCM implementations under AWGN channel is simulated and analyzed first using BPSK modulation. Also the simulation is extended to include QPSK/4PAM with bit rate 32/40Mbps, 16QAM/16PAM with 64/80Mbps, and 64QAM/64PAM with 96/120Mbps. For the wavelet-based implementation Daubechies wavelets of order 4, 6, and 8 are chosen. The simulated performance results of the implemented systems under AWGN channel are shown in Figure 5.5(a), 5.5(b) and Figure 5.6(a), 5.6(b).

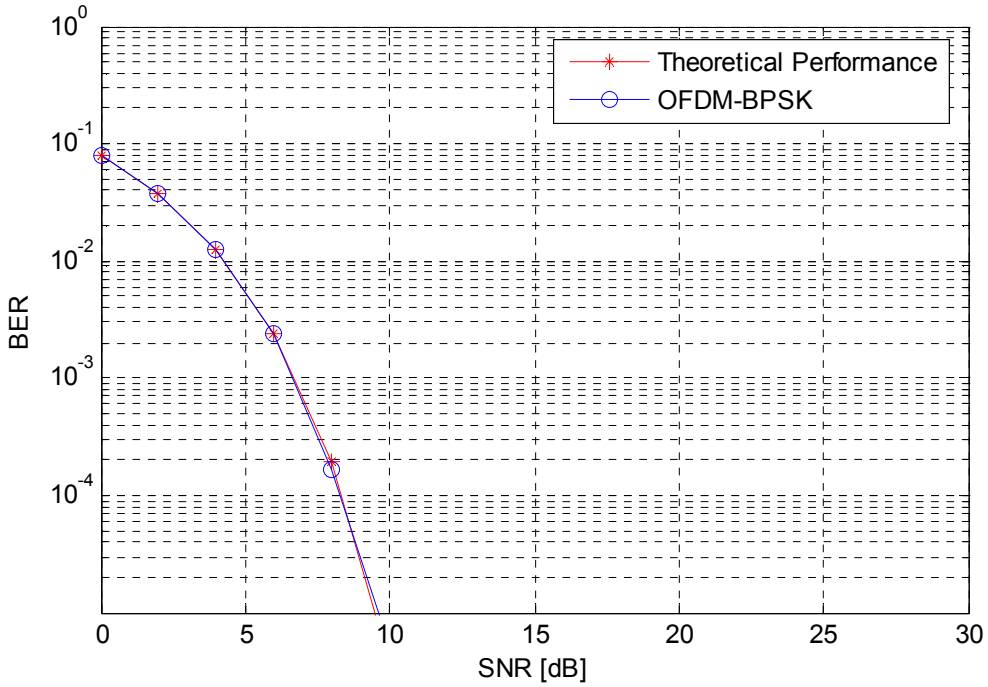

Figure 5.5(a) The AWGN channel *BER* vs. *SNR* Performance of 64-subcarrier, 16-sample cyclic prefixed DFT-based OFDM implementation for BPSK constellation.

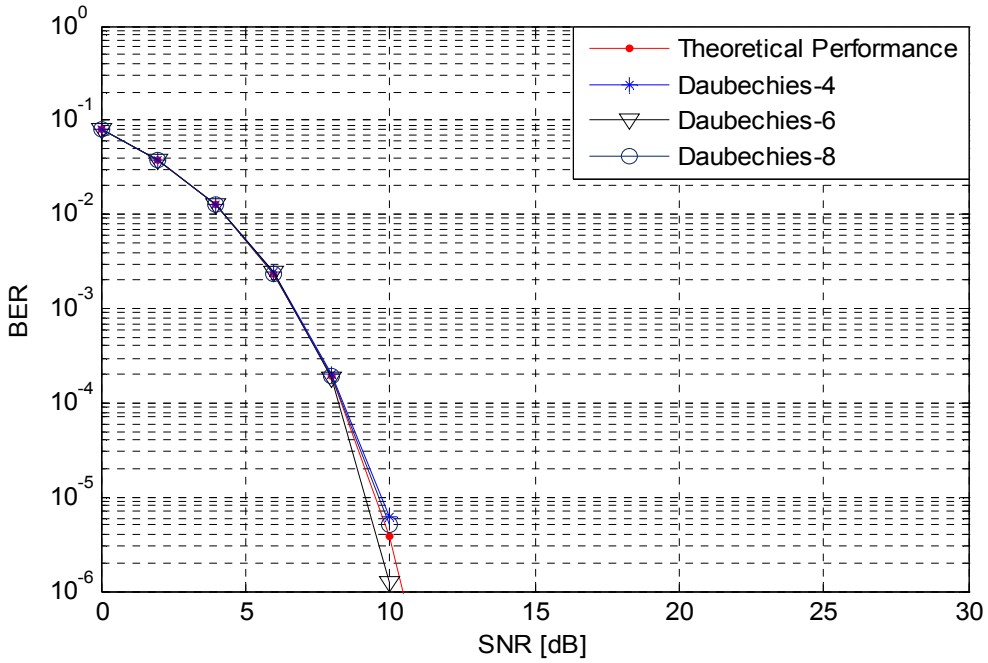

Figure 5.5(b) AWGN channel *BER* vs. *SNR* Performance of Wavelet-based OFDM scheme using Daubechies wavelet of order 4, 6, and 8 for BPSK constellation.

As it can be seen in Figure 5.5 (a) and 5.5 (b), the *BER* performance of DFT-based and DWT-based systems matches the theoretical BPSK BER performance given as

$$P_e = Q\left(\sqrt{\frac{2E_b}{N_0}}\right) \tag{5.6}$$

This basically validates the model implemented for the simulation. Furthermore the different orders of the Daubechies wavelet used for the implementation show a closely matched performance with higher order wavelets particularly Daubechies order 6 showing better performance as the SNR increases beyond 8dB which is in line with results of [60].

In comparison, the wavelet-based implementation in AWGN channel shows a slightly better *BER* performance at higher constellation sizes otherwise it is closely matched with the performance of DFT-based implementation. This close performance between the two schemes is the result of the fact that AWGN channels will not introduce *ICI* or *ISI,* as such orthogonality between the subcarriers will not be lost and this in turn ensures that the link performance to be solely dependent on the constellation size used on each subcarrier and the level of noise as seen in Figure 5.8.

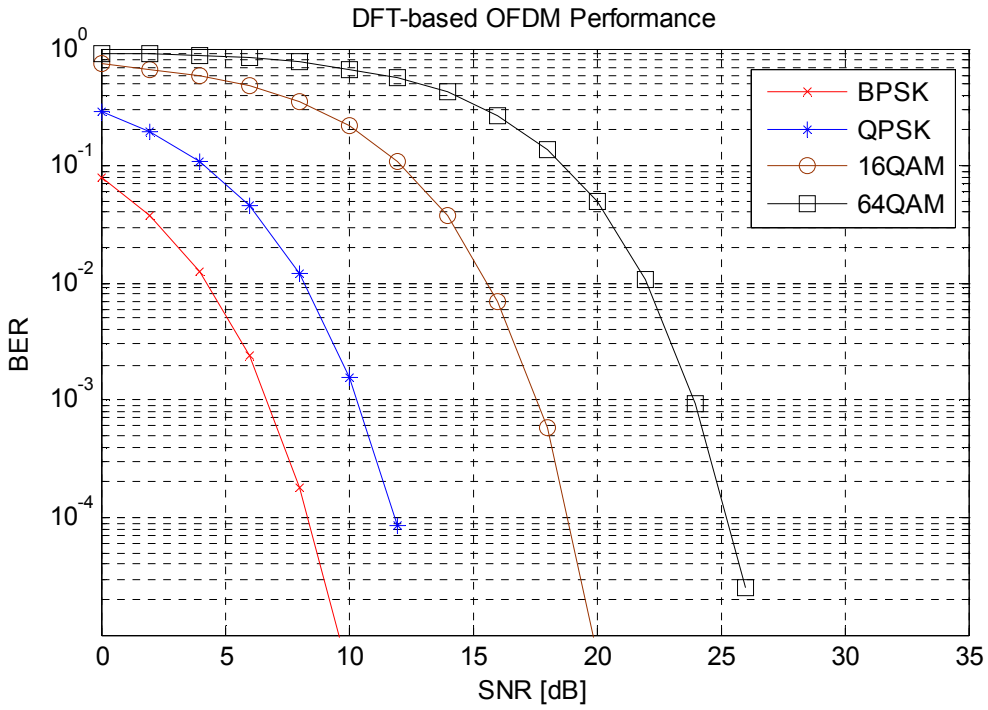

Figure 5.6(a) AWGN channel *BER* vs. *SNR* Performance of DFT-based OFDM scheme using for BPSK, QPSK, 16QAM, 64QAM constellations.

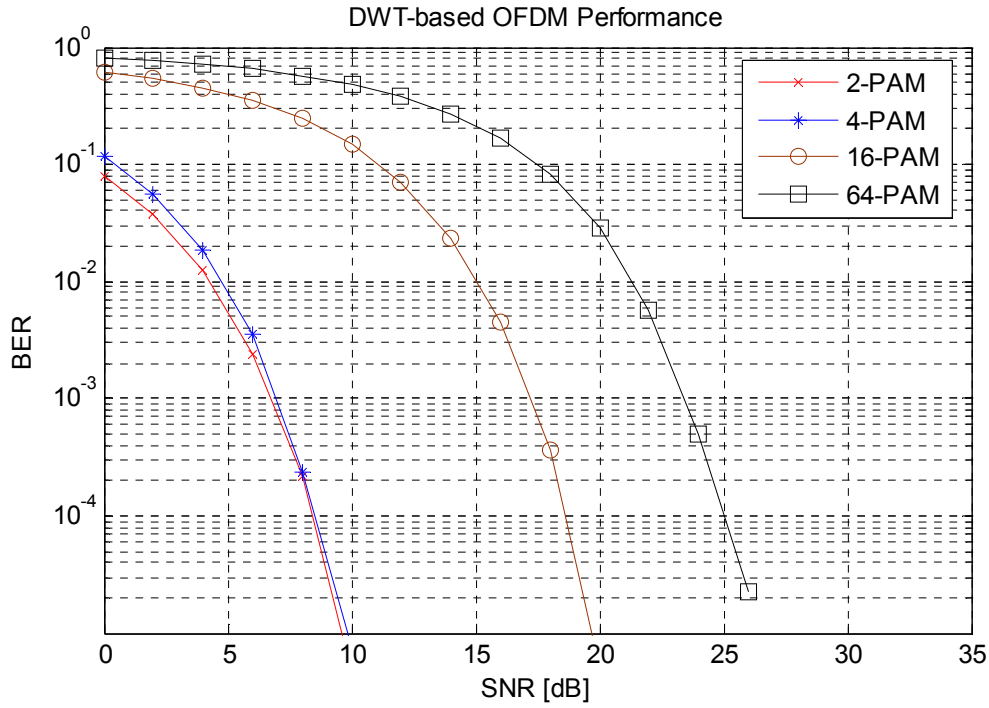

Figure 5.6(b) The AWGN channel *BER* vs. *SNR* Performance of Wavelet-based OFDM using Daubechies wavelets of order 6 for 2PAM, 4PAM, 16PAM, 64PAM.

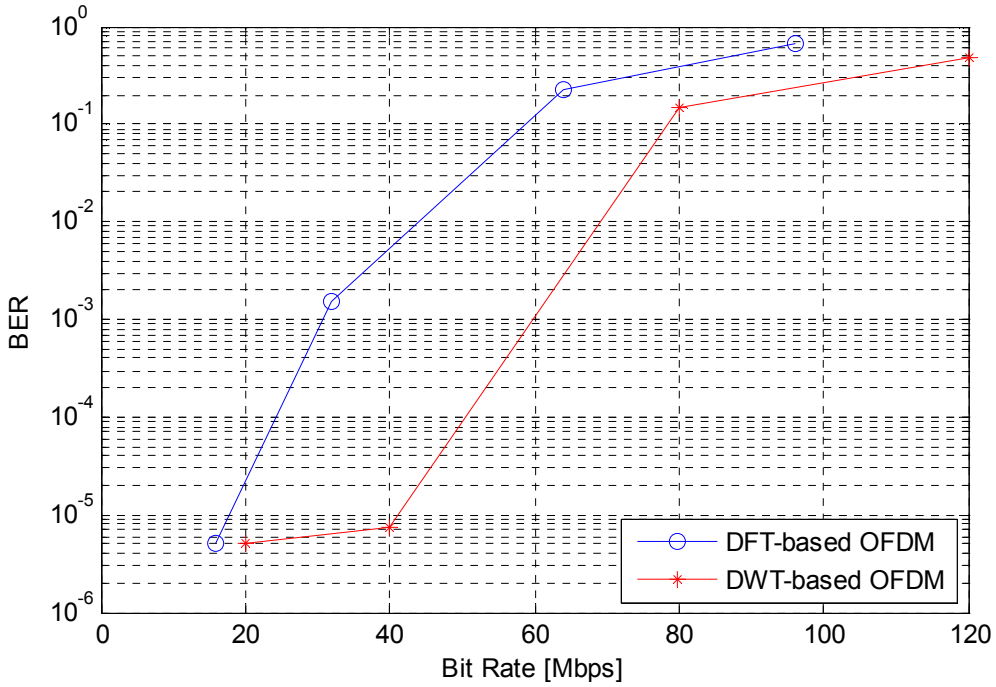

Figure 5.7 The AWGN channel OFDM *BER* vs. Bit rate performance at 10dB *SNR* for both DWT and DFT schemes.

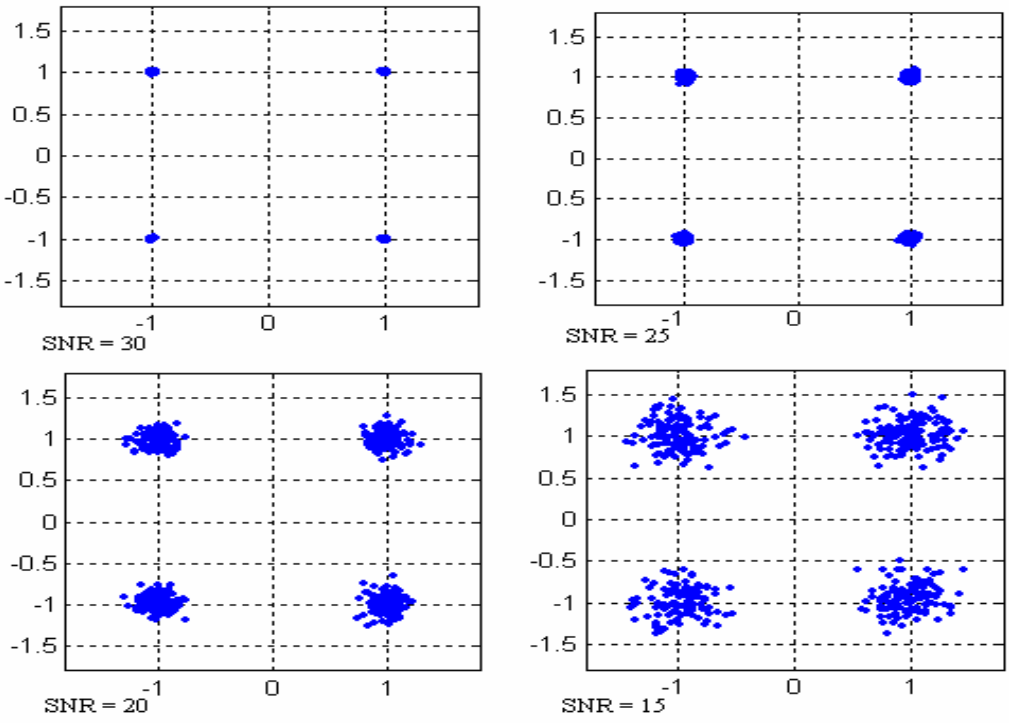

Figure 5.8 Effect of AWGN on QPSK constellation (for different noise levels)

Figure 5.7 above shows the comparison of *BER* performance of both schemes at the same 10dB signal-to-noise ratio value. The wavelet-based scheme achieves the same or better bit error rate value at higher bit rate when compared with that of the DFT-based scheme performance.

5.3. Multipath Channel Performance

Next the *BER* performance of OFDM for both DFT and Wavelet based implementations in a multipath environment is carried out. First a flat Rayleigh fading model is used to analyze the *BER* performance of the OFDM schemes. Here the difference between delays of the signals arriving through different paths is negligible, and thus the arriving signal is modeled as having only one delayed path.

Here also the DWT-based scheme is implemented at higher bit rate, 20Mbps for BPSK modulation, than that of the DFT-based implementation 16Mbps. And for that of QPSK/ 4-PAM modulation the bit rate is 32/40Mbps respectively.

The Doppler spreading is determined using the transmission carrier frequency of 5.2GHz (IEEE 802.11a WLAN). Thus simulations are performed at Doppler shift of 25Hz and 120Hz.

5.3.1 Performance in Flat Rayleigh fading channel

By using a single Rayleigh path the frequency flat fading channel is generated. The *BER* performance for both OFDM schemes using two modulation types is analyzed and the results are plotted for Doppler frequency of 25Hz and 120Hz [Figure 5.9 (a) and (b)]. The theoretical *BER* vs. *SNR* for BPSK under slowly fading Rayleigh channel is given by

$$\mathrm{Pe} = \frac{1}{2}\left(\sqrt{\frac{\gamma_b}{1+\gamma_b}}\right) \tag{5.7}$$

where $\gamma_b = \frac{\varepsilon}{N_0}$ is used as a reference for the simulation results.

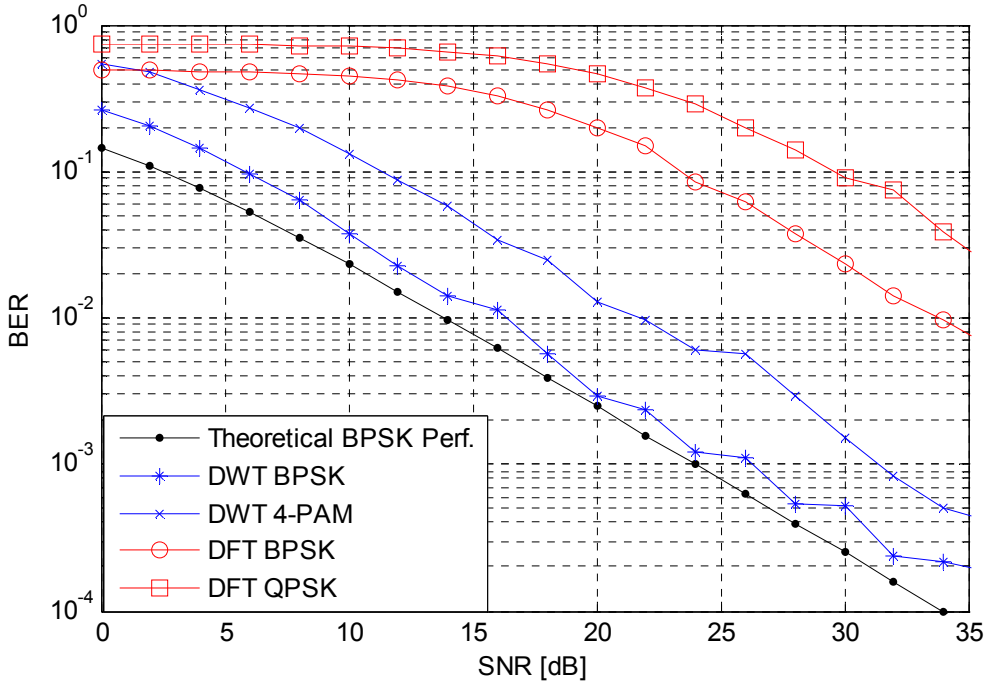

Figure 5.9(a) *BER* vs. *SNR* performance of DFT-based BPSK and QPSK and DWT-based BPSK and 4-PAM under Rayleigh fading channel (with Doppler shift of 25Hz)

The results obtained (Figure 5.9(a) and (b)) show that as the Doppler shift is increased to 120Hz the *BER* performance degrades by 2dB at a *BER* of 10^{-3}. And For both Doppler shift levels, at low *SNR* and also at high *SNR* values DWT-based implementation shows the best *BER* performance for both BPSK and 4-PAM/QPSK modulation schemes which unmatched by DFT-based implementation. Figure 5.9(a) shows that at *SNR* value of 10dB the BPSK *BER* performance of DWT-based scheme is 0.03756 while that of DFT-based scheme is 0.4442. This shows how better the wavelet-based scheme performing even if it is implemented at higher bit rate than DFT-based scheme.

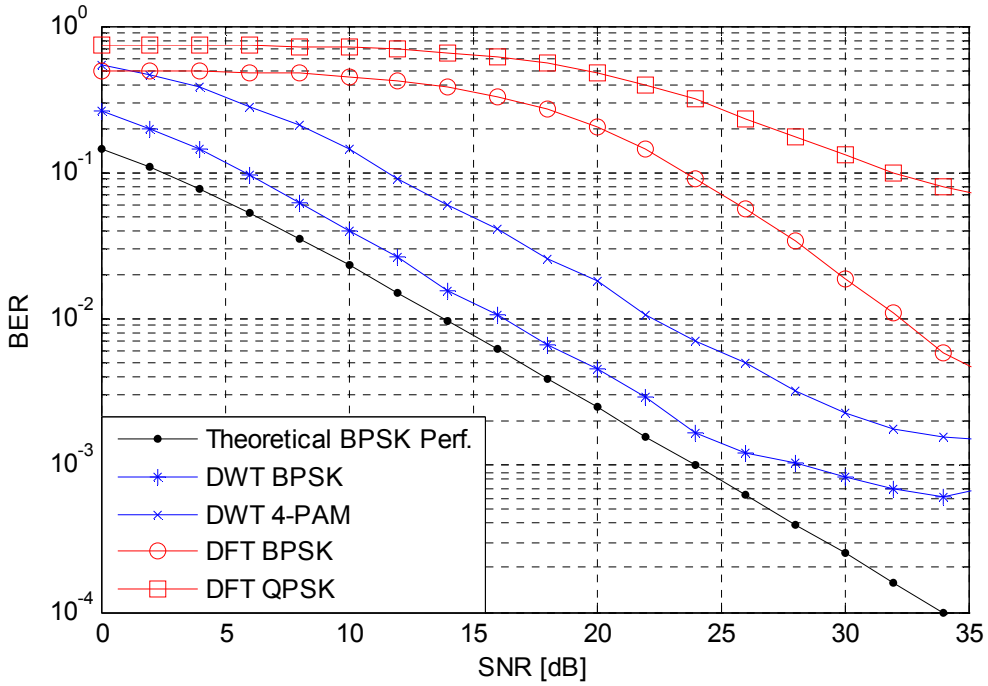

Figure 5.9(b) *BER* vs. *SNR* performance of DFT-based BPSK and QPSK and DWT-based BPSK and 4PAM under Rayleigh fading channel (with Doppler shift of 120Hz)

5.3.2 Performance in Frequency Selective Rayleigh fading channel

In practical situations the multipath components are many in number. But to carryout a plausible simulation two-path Rayleigh fading model is selected with impulse response,

$$h(n) = \delta(n) + \delta(n-p)e^{j\theta_1} \tag{5.8}$$

to generate frequency selective fading channel; where p is an integer denoting the excess delay of the channel, normalized to the symbol period of incoming data, and θ_1 is a random phase of the second path with uniform distribution over $[0, 2\pi]$.

For an indoor channel 50ns to 1.2 μs excess delays are typical. This in terms of 50ns sampling time will be and an excess delay of 1sample to 20sample. Doppler spreading effect for 25Hz is considered.

The *BER* vs. *SNR* plots for excess delay of 1 sample (in Figure 5.10(a) and 5.10(b)) indicate cyclic prefixed DFT-OFDM implementation shows improvement over that of no cyclic prefix scheme with more than 10dB at *BER* value of 2e-2. On the other hand, the wavelet-based implementation shows that all the three orders of Daubechies wavelets used perform the same at all possible *SNR* values. On these plots for *SNR* values less than 10dB for 25Hz Doppler and less than 6dB for 120HZ Doppler the wavelet-based scheme implemented at 20Mbps performs better but as the *SNR* increases it doesn't show appreciable performance improvement. While the DFT-based scheme implemented at 16Mbps shows performance improvement for higher *SNR* values.

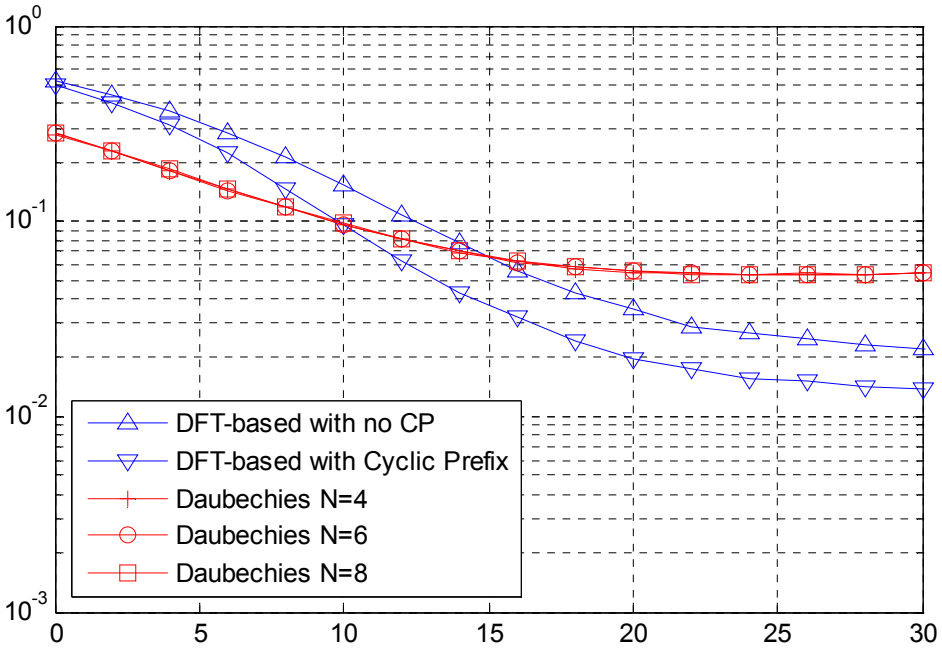

Figure 5.10 a) *BER* vs. *SNR* Performance of DFT-based with and without Cyclic Prefix and Wavelet-based, 64 subcarrier OFDM in Frequency selective Rayleigh fading channel with excess delay of 1 sample and Doppler shift of 25Hz.

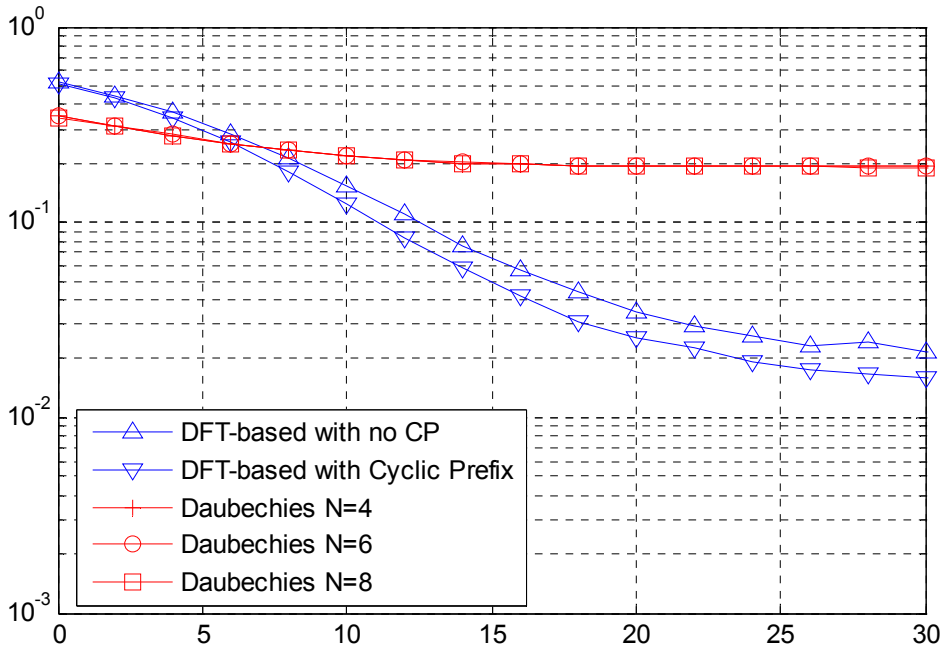

Figure 5.10 b) *BER* vs. *SNR* Performance in Frequency selective Rayleigh fading channel with excess delay of 1 sample and Doppler shift of 120Hz.

The presence of cyclic prefix with duration of 16 samples (0.8 μs) on DFT-based implementation ensures that for smaller excess delays less than half of the cyclic prefix (Figure 5.11(a) and 5.11(b)), the delay spread effect of the channel is kept within the cyclic prefix. This contributes the better performance of the DFT-based scheme over that of the wavelet-based scheme for higher *SNR* values.

As the delay spread of the channel increases the *BER* performance of DFT-OFDM degrades which finally becomes even worse than wavelet-OFDM (as seen in Figure 5.11(c)). And as for the wavelet-based implementation, the *BER* performance under different delay spread doesn't show an appreciable difference at lower Doppler shift (as seen in figures 5.10(a), 5.11(a), 5.11(b), 5.11(c)). Figure 5.11(c) shows the case of too much delay spread, which contributes to the fact that, even as the transmission *SNR* increases the *BER* performance doesn't show appreciable improvement for DFT-based scheme.

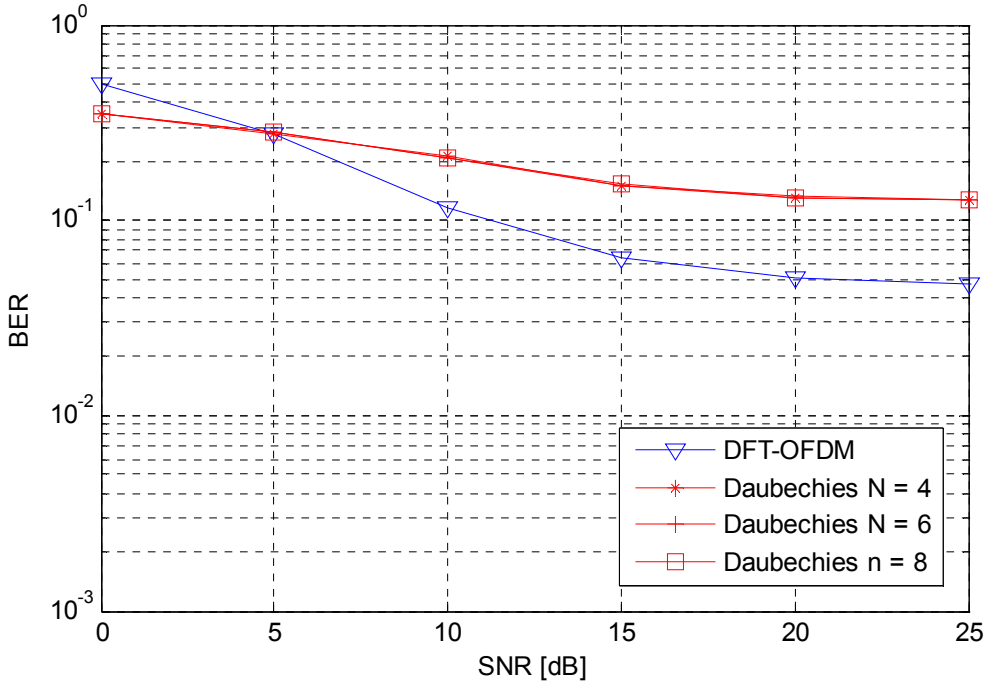

Figure 5.11 a) *BER* vs. *SNR* Performance of DFT-based with and without Cyclic Prefix and Wavelet-based, 64 subcarrier OFDM in Frequency selective Rayleigh fading channel with excess delay of 4 sample and Doppler shift of 25Hz.

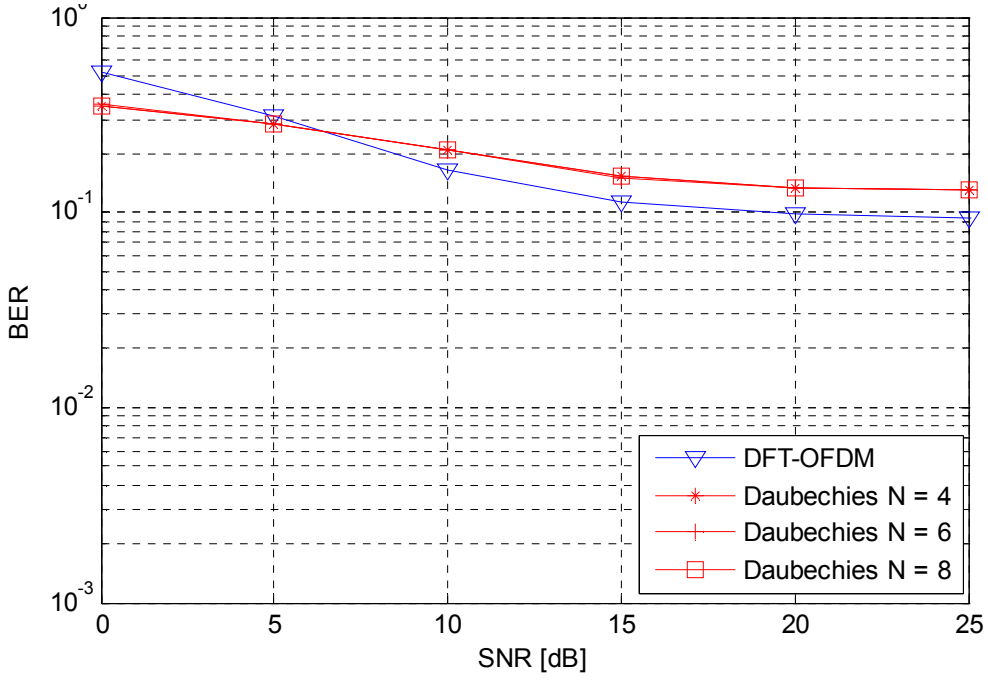

Figure 5.11 b) *BER* Performance in Frequency selective Rayleigh fading channel with excess delay of 8 sample and Doppler shift of 25Hz.

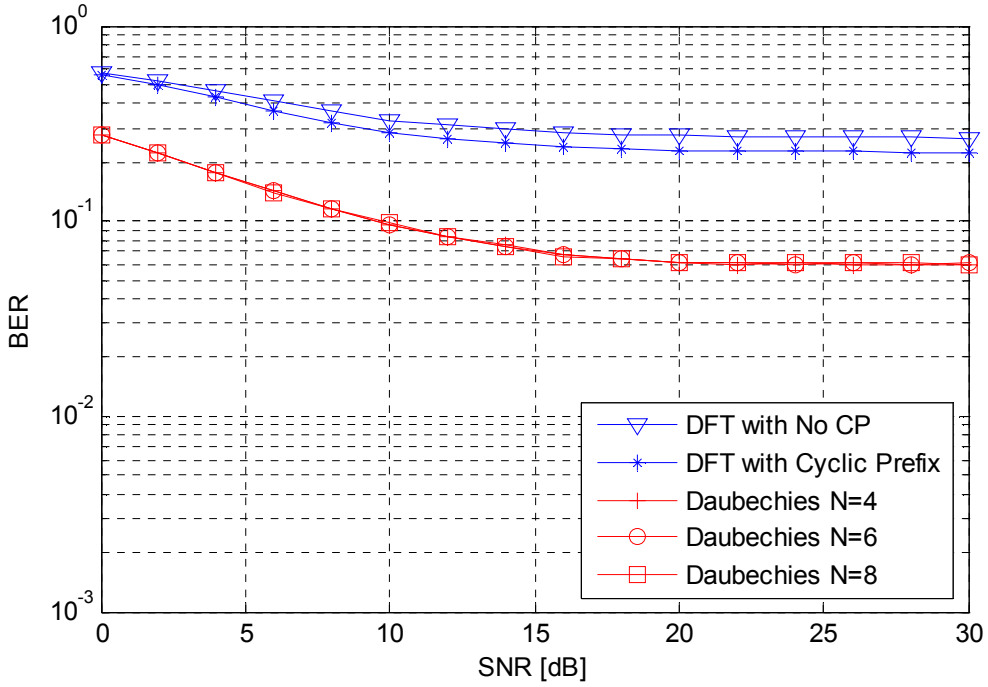

Figure 5.11 c) *BER* Performance in Frequency selective Rayleigh fading channel with excess delay of 20 sample and Doppler shift of 25Hz.

The performance comparison of the two OFDM schemes is also performed by considering the effect of no of subcarriers. The channel is frequency selective with delay spread of one sample and Doppler shift of 25Hz. And it is found that (in Figure 5.12) as the number of subcarriers increases, the BER performance gets better for every dB after an *SNR* value of 5dB, since the cyclic prefix duration increases for higher number of subcarriers.

The performance of wavelet-based implementation is shown in Figure 5.13. It shows that there is a performance gain as the number of subcarriers increases, but difference is little. This can be attributed to the fact that when the number of subcarriers increases, the frequency difference between the subcarriers decreases causing probably *ICI* to increase.

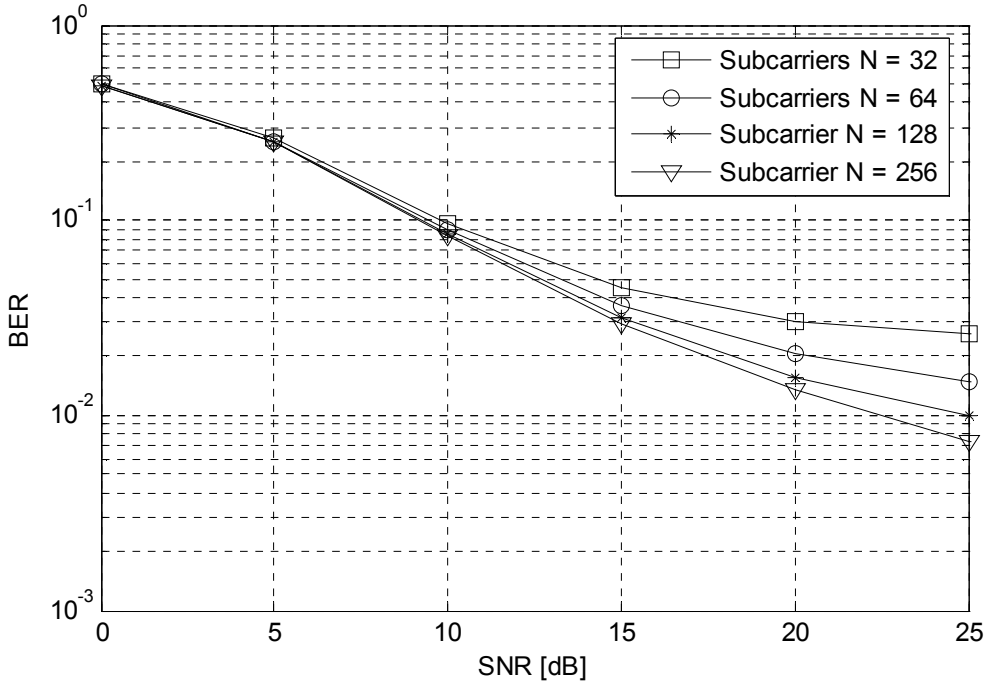

Figure 5.12 *BER* vs. *SNR* Performance of DFT-based OFDM for different subcarriers in Frequency selective Rayleigh fading channel with excess delay of 1 sample and Doppler of 25Hz.

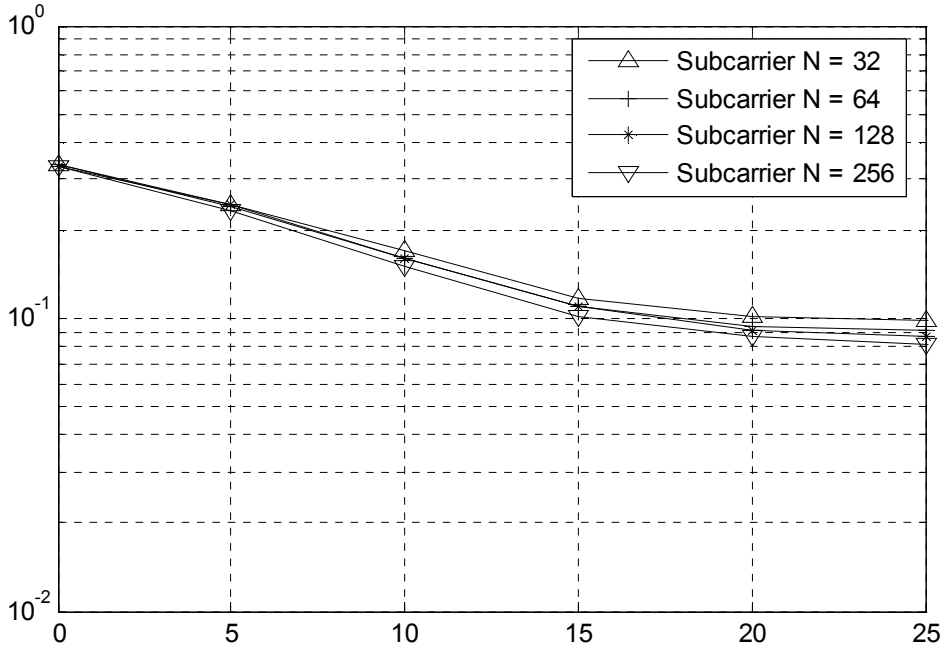

Figure 5.13 *BER* vs. *SNR* Performance of Daubechies N = 6 wavelet-based OFDM for different subcarriers in Frequency selective Rayleigh fading channel with excess delay of 1 sample and Doppler of 25Hz.

5.3.3. Effect of Carrier Frequency Offset

The effect of frequency synchronization errors has been discussed in section 3.6.2 of chapter 3. As it was said carrier frequency offset (CFO) produces frequency shift and phase rotation at the receiver affecting the orthogonality between subcarriers. The effect of CFO for different percentage of the carrier frequency under flat Rayleigh fading channel is simulated and plotted in Figure 5.14.

The resulting plot shows that increased amount of frequency error highly degrades *BER* performance of the schemes. Here for smaller amount of CFO DWT-based OFDM performance degradation is very small compared with that of DFT-based scheme. But at higher CFO the degradation of DWT-based scheme is very high.

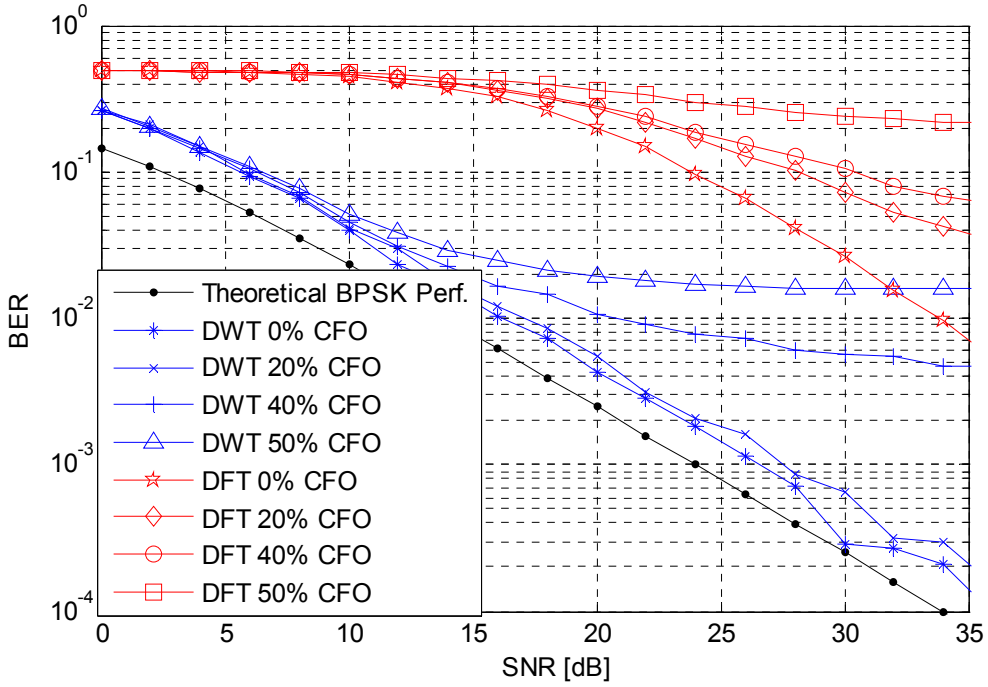

Figure 5.14 The effect of carrier frequency offset on DWT-based and DFT-based OFDM schemes under flat Rayleigh fading channel

5.4. Coded Performance

Until now the performance of OFDM system for both DFT-based and DWT-based schemes have been simulated without channel coding. Now the performance of these schemes will be simulated using channel coded bits using convolutional channel coding. The convolutional encoder will be using the industry-standard generator polynomials, $g_0 = 133_8$ and $g_1 = 171_8$, of rate R = 1/2, and constraint length k=7 as indicated in IEEE 802.11a physical standard [2] and shown in Figure 5.15.

The channel decoder will utilize hard decision viterbi algorithm. This is due to the fact that soft decision decoding involves higher computational complexity even if it gives better performance.

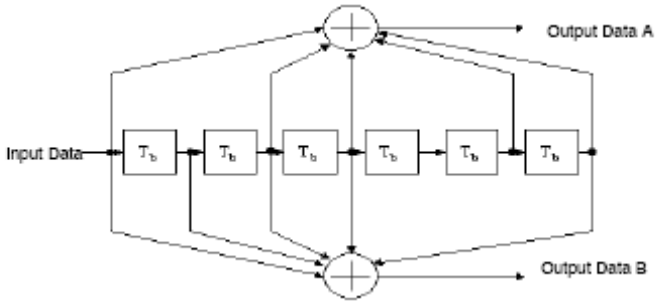

Figure 5.15 Convolutional Encoder with constraint length k=7

As the performance plot shows channel coding improves the overall link performance of the systems. The coded DWT-based scheme at a *BER* value of 10^{-3} shows on average a 6dB performance gain over the uncoded *BER* performance (Figure 5.6(a)). While the performance gain recorded for the coded DFT-based system at a *BER* value of 10^{-3} is on average 4.5dB over that of the uncoded *BER* performance (Figure 5.6(b)).

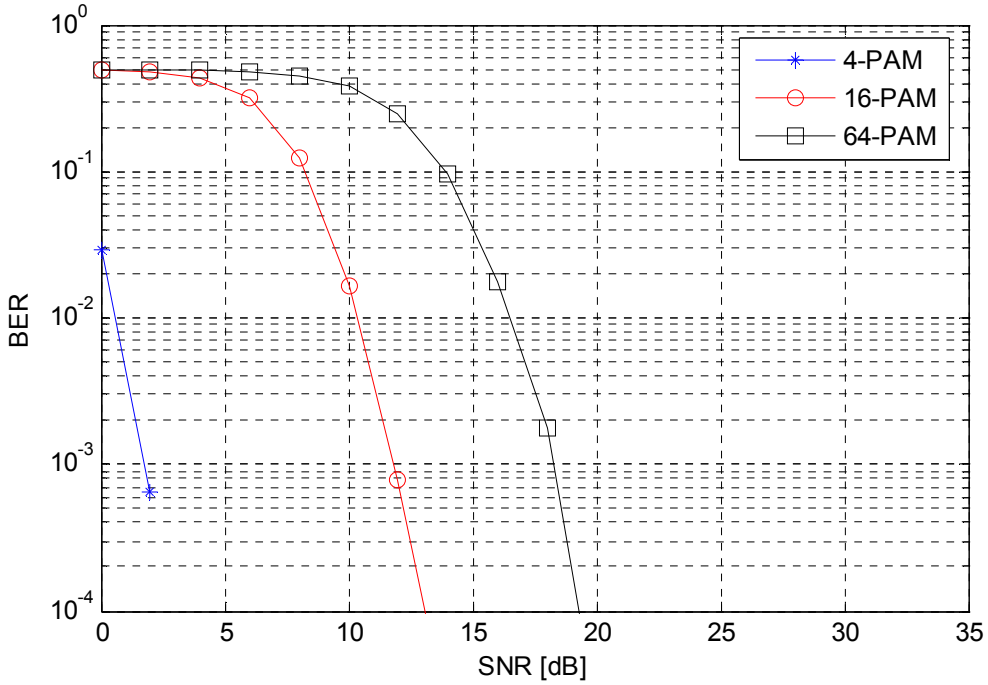

Figure 5.16(a) Coded DWT-based OFDM performance under AWGN channel

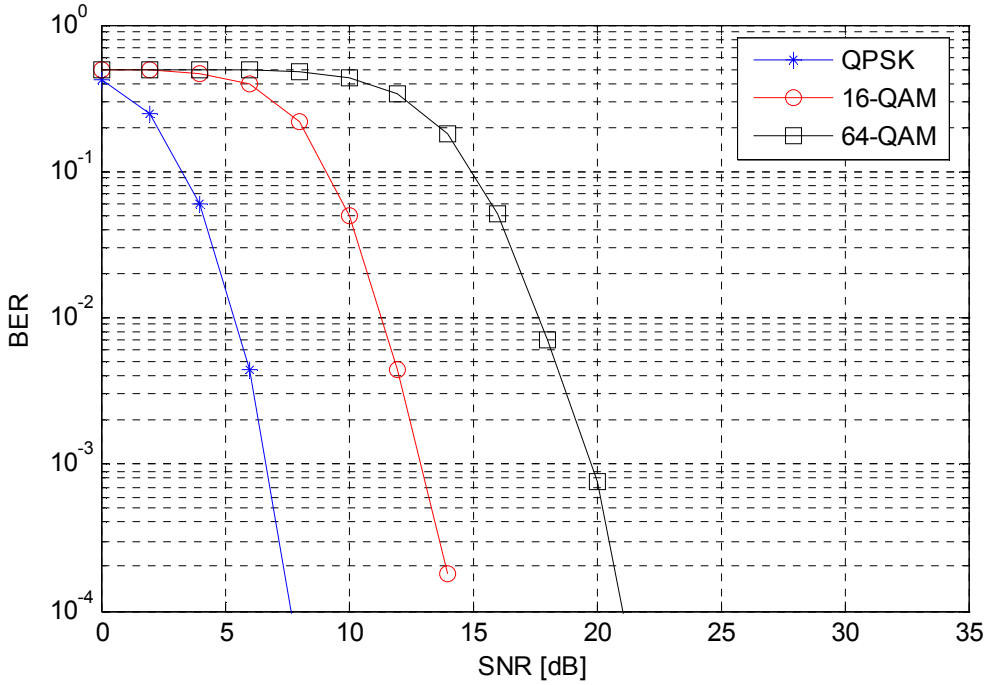

Figure 5.16(b) Coded DFT-based OFDM performance under AWGN channel

5.5. Limitations of the simulation

The implementation of the discrete wavelet transform algorithm was the biggest challenge faced while performing this thesis work. At first it showed an error floor at high SNR values which was corrected with further improvements done on the algorithm implementation and the channel models used. But still the speed of execution of the Matlab's internal FFT algorithm could not be matched.

Secondly, while the channel models used for this thesis work and also the general system implementation conform to the best trends in the area of multicarrier modulation systems research, it was not possible to show real time operation performance.

Thirdly, the effects of hardware parts such as oscillators, sampling clocks, DAC/ADC converters, up/down frequency converters on system performance of both DFT-based and DWT-based schemes could not be investigated.

Chapter 6

Conclusion and Future Work

In this thesis work we have considered two alternate ways of multicarrier modulation system implementation, discrete Fourier transform based and discrete wavelet transform based. This chapter presents concluding remarks that summarize the thesis study and suggest area for future exploration.

The work done by Zhang et al [15] is used to compare the results of the work done on this paper. On [15] the performance of DFT-based OFDM without guard band (cyclic prefix) is compared with the simplest Haar wavelet based OFDM under AWGN, flat fading and frequency selective fading channels.

On this paper it has been tried to present the wavelet based OFDM implementation using the most popular and compactly supported Daubechies wavelets. And the comparison is done with cyclic prefixed DFT-based OFDM under AWGN and flat Rayleigh fading channel, also under frequency selective fading channel at different delay spread. It has also been tried to show performance improvements of channel coding in AWGN channel, also the effects of carrier frequency offset.

6.1. Conclusion

DWT-based OFDM scheme implemented at a 25% higher bit rate was found to perform very well in AWGN and frequency flat fading channels compared with DFT-based scheme. Similar conclusion can be made about their performance for small *SNR* conditions under frequency selective channel and also when the delay spread is greater than the cyclic prefix

interval used for DFT-based scheme. While the DFT-based scheme performs better for high SNR conditions when the delay spread is less than the cyclic prefix.

The performance the different Daubechies orders used for DWT-based scheme was similar in frequency selective fading channel while it was found to have small difference in AWGN and frequency flat fading channels for high *SNR* conditions with Daubechies N = 6 performing best. And wavelet based implementation shows a better performance improvement when channel coding is used. Also it shows a better resistance to small value carrier frequency offsets.

In overall, the current status of the research is that OFDM *appears* to be a suitable technique as a modulation technique for high performance wireless telecommunications. The results obtained in this study augmented by further research might place the wavelet-based MCM system as a front runner for different communication applications.

6.2. Future Work

The study was concentrated on the basic implementation of the multicarrier modulation, as such other parameters were considered to be perfect which is not the case in real situations. So the following areas are suggested for future work:

The performance of wavelet-based OFDM may benefit from robust channel estimation and equalization algorithms optimized to wavelets. The effect of multiple transmit and receive antennas on wavelet-based MCM implementation can also be explored.

Channel coding provides performance improvement for multicarrier modulation in fading channels as suggested in the literature which may be explored in relation to wavelet-based implementation.

Performance comparison of DFT-based and DWT-based MCM schemes can also be done in multiple access applications.

References

1. J. A. C. Bingham, “Multicarrier Modulation for Data Transmission: An Idea Whose Time Has Come,” *IEEE Communications Magazine*, pp. 5-14, May 1990.
2. IEEE Std 802.11a-1999(R2003): Part 11: Wireless LAN Medium Access Control (MAC) and Physical Layer (PHY) specifications; High-speed Physical Layer in the 5 GHz Band, *IEEE*, 1999.
3. ETSI TS 101 475 V1.1.1 (2000-04): Broadband Radio Access Networks (BRAN); HIPERLAN Type 2; Physical (PHY) Layer, http://www.etsi.org/tb/status/
4. F. Ohrtman, “WiMAX Handbook Building 802.16 Wireless Networks,” McGraw-Hill, USA, 2005.
5. Final draft ETSI EN 300 401 V1.4.1 (2006-01): Radio Broadcasting Systems Digital; Audio Broadcasting (DAB) to mobile, portable and fixed receivers, http://www.etsi.org/tb/status/
6. ETSI EN 300 744 V1.4.1 (2001-01): Digital Video Broadcasting (DVB); Framing structure, channel coding and modulation for digital terrestrial television, http://www.etsi.org/tb/status/
7. S. B. Weinstein and P. M. Ebert, “Data transmission by frequency division multiplexing using discrete Fourier transform,” *IEEE Transactions on Communication Technology*, Vol. Com-19, pp. 628-634, October 1971.
8. A. Peled and A. Ruiz, “Frequency domain data transmission using reduced complexity algorithms,” *IEEE International Conference Acoustics, Speech, Signal Processing ICASSP* '80, (Denver, CO), pp. 964-967, 1980.
9. L. J. Cimini, Jr., “Analysis and Simulation of a Digital Mobile Channel Using Orthogonal Frequency Division Multiplexing,” *IEEE Transactions on Communication*, Vol. COM-33, No.7, pp. 665-675, July 1985.

10. B. R. Saltzberg, "Performance of an efficient parallel data transmission system," *IEEE Transactions on Communications*, vol. COMM-15, pp. 805-811, December 1967.
11. H. Steendam and M. Moeneclaey, "Analysis and Optimization of the Performance of OFDM on Frequency-Selective Time-Selective Fading Channels," *IEEE Transactions on Communication*, Vol. 51, No.12, pp. 1811-1819, December 1999.
12. Y. H. Kim, I. Song, H. G. Kim, "Performance Analysis of a Coded OFDM System in Time-Varying Multipath Rayleigh Fading Channels," *IEEE Transaction on Vehicular Technology*, Vol. 48, No. 5, pp. 1610-1615, September 1999.
13. S. D. Sandberg and M. A. Tzannes, "Overlapped Discrete Multitone Modulation for High Speed Copper Wire Communications," *IEEE Journal on Selected Areas in Communications*, Vol. 13, No. 9, pp. 1571-1585, December 1995.
14. W. Kozek, G. Pfander, J. Ungermann, G. Zimmermann, "A Comparison of Various MCM Schemes," 5th International OFDM-Workshop, Hamburg, Germany, 2000.
15. H. Zhang, D. Yuan, M. Jiang, D. Wu, "Research of DFT-OFDM and DWT-OFDM on Different Transmission Scenarios," *Proceedings of 2nd International Conference on Information Technology and Applications ICITA*, 2004.
16. W. C. Jakes, Jr., Ed., "Microwave Mobile Communications," pp. 11-131, Wiley and Sons, New York, USA, 1974.
17. B. Sklar, "Digital Communications: Fundamentals and Applications," pp. 945-1011, Prentice Hall, Englewood Cliffs, USA, 1988.
18. A. Goldsmith, "Wireless Communications," pp. 350-377, Cambridge University Press, Cambridge, 2005.
19. B. Sklar, "Rayleigh Fading Channels in Mobile Digital Communication Systems Part I: Characterization," *IEEE Communications Magazine*, July 1997.
20. K. Brayer, Ed., "Data Communications via Fading Channels," IEEE Press, New York, USA, 1975.
21. H. Hashemi, "The Indoor Radio Propagation Channel," *Proceedings of the IEEE*, Vol. 81, No. 7, July 1993.
22. J. G. Proakis, "Digital Communications," 4th Ed., McGraw-Hill, New York, USA, 2003.

23. P. A. Bello, "Characterization of Randomly Time-Variant Channels," *IEEE Transactions on Communications Systems*, December 1963.
24. A. Papoulis, S. U. Pillai, "Probability, Random Variables and Stochastic Processes," 4th Ed., McGraw-Hill, New York, USA, 2002.
25. B. L. Floch, M. Alard and C. Berrou, "Coded Orthogonal Frequency Division Multiplex," *Proceedings of the IEEE*, Vol. 83, No, 6, pp. 983-997, June 1995.
26. X. Cai, G. B. Giannakis, "Bounding Performance and Suppressing Intercarrier interference in Wireless Mobile OFDM," *IEEE Transactions on communications*, Vol. 51, No. 12, pp. 2047-2056, December 2003.
27. R. Schafer and A. Oppenheim, "Discrete-time Signal Processing," Prentice-Hall, Englewood Cliffs, USA, 1989.
28. W. Henkel, G. Taubock, P. Odling, P. O. Borjesson, N. Petersson, "The cyclic Prefix of OFDM/DMT – An Analysis," *IEEE International Seminar on Broadband Communication*, Zurich, 2002.
29. J. D. Bakker, "Eliminating The OFDM Cyclic Prefix," *Proceedings of the IEEE International Conference on Personal Indoor and Mobile Radio Communications PIMRC,* 2002.
30. M. R. D. Rodrigues, "Modeling and Performance Assessment of OFDM Communication Systems in the presence of Non-linearities," PhD dissertation, University College London, England, 2002.
31. Ramjee Prasad, "OFDM for Wireless Communication Systems," pp. 117-147, Artech House, Boston, USA, 2004.
32. V. D. Nguyen, H.-P. Kuchenbecker, "Intercarrier and Intersymbol Interference Analysis of OFDM Systems on Time-Invariant Channels," *Proceedings of the IEEE International Conference on Personal Indoor and Mobile Radio Communications PIMRC,* 2002.
33. B.-L. P. Chaung, "Simulation of Adaptive Array algorithms for OFDM and Adaptive Vector OFDM systems," MSc Thesis, Virginia Polytechnic Institute and State University, USA, 2002.

34. E. Lawrey, C. J. Kikkert, "Peak to Average Power Ratio Reduction of OFDM Signals using Peak Reduction Carriers," *Fifth International Symposium on Signal Processing and its Applications ISSPA'*99, Brisbane, Australia, August, 1999.
35. K. R. Panta, J. Armstrong, "Effects of Clipping on the Error Performance of OFDM in Frequency Selective Fading Channels," *IEEE Transactions on Wireless Communications*, VOL. 3, No. 2, March 2004.
36. N. Dinur, D. Wulich, "Peak-to-Average Power Ratio in High Order OFDM," *IEEE Transactions on Communications,* VOL. 3, No. 2, pp. 1063-1072, June 2001.
37. D. Declercq and G. B. Giannakis, "Peak to Average Ratio Reduction for Multicarrier Transmission: a Review," www.citeseer.ist.psu.edu/617547.html .
38. I. Jeanclaude, H. Sari, and G. Karam, "Transmission Techniques for digital Terrestrial TV Broadcasting," *IEEE Communication Magazine*, Vol. 33, No. 2, pp 100-109, Feb. 1995.
39. T. Keller, L. Piazzo, P. Mandarini, and L. Hanzo, "Orthogonal Division Multiplex Synchronization Techniques for Frequency-Selective Fading Channels," *IEEE Journal on Selected Areas in Communications*, Vol. 19, No. 6, June 2001.
40. M. Sandell, J.-J. Van de Beek, P. O. Borjesson, "Timing and Frequency synchronization in OFDM systems Using the Cyclic Prefix," *In Proceedings of International Symposium on Synchronization*, pp. 16-19, Essen Germany, December, 1995.
41. S. Coleri, M. Ergen, A. Puri, A. Bahai, "A Study of Channel Estimation in OFDM Systems," *Proceedings of the IEEE Vehicular Technology Conference*, September 2002.
42. S. Coleri, M. Ergen, A. Puri, A. Bahai, "Channel Estimation Techniques Based on Pilot Arrangement in OFDM Systems," *IEEE Transactions on Broadcasting*, Vol. 48, pp. 223-229, September 2002.
43. P. Frenger, A svensson, "A Decision Directed Coherent Detector for OFDM," *Proceedings of the IEEE Vehicular Technology Conference*, April/May 19965.
44. J.-J. van de Beek, O. Edfors, M. Sandell, S. K. Wilson and P. O. Börjesson, "On channel estimation in OFDM systems," *Proceedings of the IEEE Vehicular Technology Conference*, vol. 2, pp. 815-819, July 1995.

45. O. Edfors, M. Sandell, J.-J. van de Beek, S. K. Wilson and P. O. Börjesson, "Analysis of DFT-based Channel Estimators for OFDM," Lulea University of Technology, Research Report TULEA, Vol. 17, 1996.
46. O. Edfors, M. Sandell, J.-J. van de Beek, S. K. Wilson and P. O. Börjesson, "OFDM channel estimation by singular value decomposition," *Proceedings of the IEEE Vehicular Technology Conference*, Vol. 2, pp. 923-927, April/May 1996.
47. B. Muquet, M. de Courville, P. Duhamel, "Subspace-Based Blind and Semi-Blind Channel Estimation for OFDM Systems*," IEEE Transactions on Signal Processing*, Vol. 50, No. 7, pp. 1699-1712, July 2002.
48. T. Keller and L. Hanzo, "Adaptive Multicarrier Modulation: A Convenient Framework for Time-Frequency Processing in Wireless Communication," *Proceedings Of The IEEE*, VOL. 88, NO. 5, May 2000.
49. A. Cohen and J. Kovacevic, "Wavelets: The Mathematical Background," *Proceedings Of The IEEE*, April 1996.
50. Amara Graps, "An Introduction to Wavelets," *IEEE Computational Science and Engineering,* Vol. 2, No. 2, pp. 50-61, Summer 1995.
51. M. Vettereli, J. Kovacevic, "Wavelets and subband Coding," Prentice-Hall, New Jersey, USA, 1995.
52. Anthony Teolis, "Computational Signal Processing with Wavelets," Birkhauser, Boston, USA, 1998.
53. N. Hess-Nielsen, M. V. Wickerhauser, "Wavelets and Time-Frequency Analysis," *Proceedings of the IEEE*, Vol. 84, No, 4, pp. 523-540, April 1996.
54. K. Ramchandran, M. Vittereli, C. Herley, "Wavelets, Subband coding, and Best Bases," *Proceedings of the IEEE*, Vol. 84, No, 4, pp. 541-560, April 1996.
55. A. N. Akansu, M. V. Tazebay, M. J. Medley, P. K. Das, "Wavelet and Subband Transforms: Fundamentals and Communication applications," *IEEE Communications Magazine*, pp. 104-115, December 1997.
56. Heather M. Newlin, "Developments in The Use of Wavelets in Communication Systems," *Proceedings of the IEEE Millennium Communications Conference*, Vol. 1, pp. 343-349, October 1998**.**

57. A. Jamin, P. Mahonen, “Wavelet Packet Modulation for Wireless Communications,” *Journal Of Wireless Communications and Mobile Computing*, Vol. 5, Issue 2, March 2005.
58. J. C. Van Den Berg, “Wavelets in Physics,” Cambridge University Press, Cambridge, UK, 1999.
59. S. G. Mallat, “Multifrequency channel decompositions of images and wavelet models,” *IEEE Transactions on Acoustics, Speech and Signal Processing*, Vol. 37, No. 12, pp. 2091-2110, 1989.
60. B.G. Negash and H. Nikookar, “Wavelet Based OFDM for Wireless Channels,” *IEEE Vehicular Technology Conference*, pp. 688-691, 2001.
61. M.L. Doelz, E.T. Heald, D.L. Martin, “Binary Data Transmission Technique for linear systems,” *Proceedings of IRE*, Vol. 45, pp. 656-661, May 1957.
62. Phillip A. Bello, “Selective fading limitations of the Kathryn modem and some system design considerations,” *IEEE Transactions on Communications Technology*, Vol. com-13, pp. 320-333, Sept. 1965.
63. Mark Zimmerman and Alan Kirsch, “The AN/GSC-10 (Kathryn) variable rate data modem for HF radio,” *IEEE Transactions on Communications Technology*, Vol. com-16, pp. 197-205, April 1967.
64. R.W. Chang, “Synthesis of Band-limited Orthogonal Signals for Multichannel Data Transmission,” Bell Systems Technology Journal, Vol. 45, pp. 1775-1796, Dec. 1996.
65. Gregory W. Wornell, “Emerging Applications of Multirate Signal Processing and Wavelets in digital Communications,” *Proceedings of the IEEE*, Vol. 84, No, 4, pp. 586-603, April 1996.
66. M. Vettereli and Cormac Herley, “Wavelets and Filter Banks: Theory and Design,” *IEEE Transactions on Signal Processing*, Vol. 40, No. 9, pp. 2207-2232, Sept. 1992.

Declaration

I, the undersigned declare that this thesis is my original work, and has not been presented for a degree in this or any other university, and all sources of materials used for the thesis have been fully acknowledged.

Sinshaw Bekele	_____
Name	Signature
Addis Ababa	January 2007
Place	Date of submission

This thesis has been submitted with my approval as a university advisor

Dr.-Ing. Hailu Ayele	_____
Advisor Name	Signature